On Architecture and Scalability of Optical Multi-Protocol Label Switching Networks Using Optical-Orthogonal-Code Label

WEN Yonggang

A Thesis Submitted in Partial Fulfillment

Of the Requirements for the Degree of

Master of Philosophy

In

Information Engineering

June 2001


香港中文大學
大學
圖書館系統
22 APR 2002
UNIVERSITY
LIBRARY SYSTEM
THE CHINESE UNIVERSITY OF HONG KONG

Acknowledgement

Foremost, I would like to express my warmest gratitude toward my research supervisor, Prof. Lian-Kuan Chen, for his guidance and support in my research and studies. I was introduced to the field of Optical Communications by his generous offer that supports my research and living in Hong Kong. His working attitude and research ethics have been inspirational to me.

I would like to express my deepest appreciation to Prof. Frank Tong and Dr. Calvin Chan, for their illuminating directions. During my last two-year research and study in the Chinese University of Hong Kong, they gave me so much help in experiment-doing, paper-writing and other things.

Moreover, I would like to thank Prof. Ricky Ho, who is now on leave from the Chinese University of Hong Kong. His hardworking and exaction in research set a good example for me. I owe much to his kind help in my first paper published on Journal of Lightwave Technology.

Furthermore, I would like to thank my colleagues from the Lightwave Communications Lab, Dr. Simon Chan, Mr. Eddie Kong, Mr. Kit Chan, Mr. Vincent Hung, Mr. Arthur Cheung, Mr. Wu Jisong and Ms. Zhang Yu, for their help and encouragement in my work.

I would like to acknowledge the Information Engineering Department staff for their kind support, and my friends in the Chinese University of Hong Kong, Mr. Yu Haitao, Mr. Yang Yang, Mr. Yang Qin, and Mr. Hu Ke, for their friendly help and making my stay enjoyable.

Most of all, I wish to thank my father, mother and sister for their support and encouragement. This thesis is dedicated to my parents.

Abstract

In this thesis, an optical MPLS network using OOC as label has been proposed with the architecture of core router based on all-optical code conversion. The fundamental limits on scalability of the proposed core router, including the label capacity and the switch cascadability, have been investigated with derived closed-form solutions.

The first part of the thesis presents the detail of implementing the all-optical OMPLS core router. It has a four-stage architecture: decoder, threshold device, optical space switch and encoder.

The second part of the thesis investigates the scalability of the photonic OOC-based MPLS network. For the proposed core router, the cascadability could be degraded by the non-ideal performance of the optical space switch and the TGIT device. For example, the finite crosstalk suppression ratio (ε) of the optical space switch induces inter-channel coherent and incoherent crosstalk, and the limited on/off ratio (α) of the TGIT device induces the residue intensity of MAI and sidelobes. In this part, the detrimental effects of the finite crosstalk suppression ratio (ε) of the optical space switch and the limited on/off ratio (α) of the TGIT device are investigated. By the criteria of 1-dB power-penalty and 5% residue intensity, the numerical simulations show that the network can support up to 20 consecutive nodes for 64-label (8-wavelength, 8-code) switch fabric with 45-dB crosstalk suppression.

摘要

本论文提出了一种用正交码（OOC）做标签（Label）的光多协议标签交换（MPLS）网络，它的核心路由器（Core Router）是基于全光码变换（Code Conversion）技术的。同时，本论文以显式表达式的方式讨论了核心路由器在可扩展性（Scalability）方面的受到限制，包括标签的容量（Label Capacity）和交换机的级连性（Switch Cascadability）。

本文的第一部分讨论了全光 MPLS 路由器的实现。这种路由器是一个四级的结构：解码器，门限设备，光交换机和编码器。

本文的第二部分讨论了光 MPLS 网络的可扩展性。就我们提出的核心路由器，它的级连性可以受到光交换机（Optical Space Switch）和门限设备（TGIT）的非理想工作状态的限制。例如，光交换机的有限交叉抑制率（Crosstalk Suppression Ratio）导致信道间的干扰（Inter-channel Crosstalk）和无关干扰（Incoherent Crosstalk），门限装置的有限的开关率（on/off Ratio）导致残存的 MAI 和副瓣。在本部分，我们着重讨论了光交换机的有限交叉抑制率和门限装置的有限的开关率带来的有害作用。 由 1-dB Power Penalty 和 5%残存强度的标准，数值模拟显示：对于一个 64 个标签（8 个波长，8 个码字）和 45-dB 交叉干扰的系统，可以连续级连的节点可达 20 个。

Contents

List of Figures

Chapter 1

Introduction

1.1 Multi-Protocol Label Switching (MPLS) Technology

The continuous explosive growth in Internet traffic has triggered a surge in bandwidth requirement, both in long haul network and in metro/access network. With the huge capacity of optical fiber, emerging wavelength-division-multiplexing (WDM) technology can meet this bandwidth requirement. Proposed as a means to dramatically increase the transmission capacity in a single fiber originally, WDM network designs have been evolved to include other desirable features, such as, protocol transparency, dynamic reconfigurability, and improved survivability [1-5,10], outperforming the traditional SDH/SONET networks.

Meanwhile, there are several major trends in designing a robot WDM network. These are: (1) Dynamic bandwidth/wavelength provisioning ; (2) Interoperability between vendors/service providers; (3) Intelligent optical routing/signaling; (4) Rings to mesh architecture; (5) Ultra long distance transmission line and (6) collapse of protocol stack. Among them, the most important is that emerging WDM networks need to support intelligent optical routing and switching. For this purpose, efficient routing can be achieved by collapsing of the protocol stacks [6].

As shown figure 1.1(a), traditionally, network designers incorporate several standard layers (IP over ATM over SONET/SDH over Optical) to implement optical systems. Collapse of these layers can enhance WDM network to provide protocol transparency, dynamic recofigurability and improved survivability. In Figure 1.1, two alternative approaches based on multi-protocol label switching (MPLS) technology are proposed for the collapse of protocol stacks.

Figure 1.1(b) shows the layer stack of the first one using the combination of IP and MPLS over optical layer. The combination of IP and MPLS over optical layer promises interoperability and End-to-End QoS, and the optical layer provides high

capacity transport, reliable transport and bandwidth management. Based on current technology, routers based on Internet Protocol/multi-protocol label switching (IP/MPLS) are now reaching capacities in the sub-terabit-per-second throughput range, with 10 Gb/s line cards. To reach multi-terabits-per-second throughputs, massive parallelism and complex interconnection are proposed. Although probably feasible in the medium term as claimed by several vendors for a third generation of router [6], they are not likely to drive the cost down significantly. However, this approach has the advantage of being completely IP-driven, and therefore obviously compatible with traffic engineering and distributed management techniques developed for IP networks.

The other approach shown in Figure 1.1(c) incorporates MPLS in optical layer, and provides OMPLS interface for upper layer, such as, IP layer. For this approach, the optical layer can be partitioned into two basic components: (1) optical switches for direct cross-connection of optical channels without electrical demultiplexing, and (2) MPLS-based control plane, for enhanced management flexibility. This scheme has great potential as it makes simplified forwarding and all-optical label swapping possible. Moreover, application of OMPLS techniques, which allows transport of IP over service-sensitive lower-layer technologies and switching of MPLS on top of optical crossconnects for dynamic resource allocation, provides some flexibility and agility in the redistribution of resources along the network. Thus, it performs better in coping with the massive traffic pattern variations that core networks experience over long periods of time.

To accommodate data traffic in WDM packet-based network, slim protocol stacks with flexible bandwidth-on-demand and dynamic reconfigurability features are designed [7]. In these designs, the second approach (optical multi-protocol label switching (OMPLS) technique) is employed to allow efficient packet forwarding while decoupling the packet routing and forwarding operations to support multiple-routing services [8]. OMPLS also extends beyond the traditional IP forwarding function, and has many advantages including simplified forwarding, efficient explicit

routing, traffic engineering and QoS routing. Most likely, OMPLS will be used as a unifying network management and traffic engineering protocol for a variety of transport systems, thus also extended as Generalized Multi-Protocol Label Switching (GMPLS) [9].

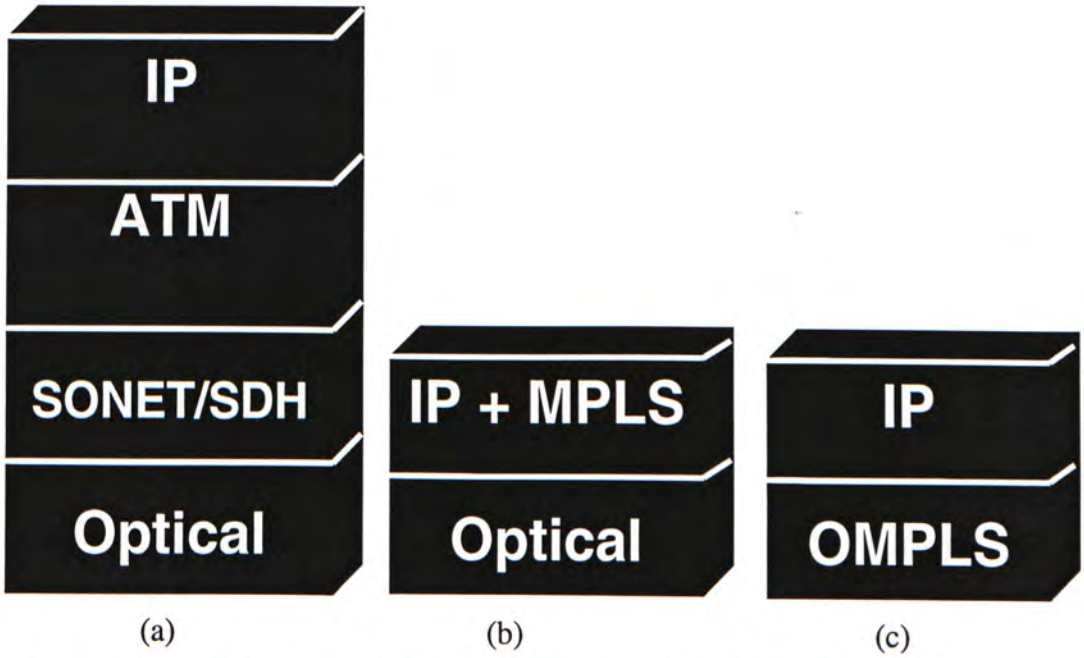

Figure 1.1 Protocol stack solutions for transport of IP-over-WDM networks. (a) Traditional approach, (b) IP/MPLS approach, and (c) IP over OMPLS approach.

1.2 Objective of this Thesis

The architecture issues and the scalability of optical multiprotocol label switching (OMPLS) networks using optical orthogonal codes (OOC) as labels are investigated in this thesis. The thesis is organized as follows.

Chapter 1: Introduction

This chapter describes some network trends that meet the rapid growth of the bandwidth requirement. The promising trend is the collapse of stacks. There are two approaches to incorporate optical layer and MPLS into WDM networks for intelligent optical routing/signaling: IP/MPLS and IP-over-OMPLS.

Chapter 2: Optical MPLS Network and Optical Label Schemes

This chapter describes a generic photonic MPLS network and its layer infrastructure. With this infrastructure, an overview of four primary optical MPLS technologies is given in this chapter. These are (1) time-division label scheme, (2) wavelength-division label scheme, (3) frequency-division label scheme and (4) code-division label scheme.

Chapter 3: Architecture of OOC-based OMPLS network

The architecture issues of the generic OOC OMPLS network are described in this chapter. First, the fundamental idea of OOC OMPLS is given. Then, we will focus on the most important component of this network, a four-stage code converter for core router. Finally, the various implementations of every individual stage of the code converter are outlined and compared. There are encoders/decoders, threshold device and optical space switch fabric.

Chapter 4: Scalability of OOC-based OMPLS network

The fundamental limits on the scalability of optical multi-protocol label switching (OMPLS) networks using optical orthogonal codes (OOC) as labels are investigated in this chapter. Based on the proposed four-stage architecture of the optical core router, closed-form results for the label switching capacity and the network

cascadability are derived. Originated from the intrinsic uni-polar property of OOC, the multi-access interference (MAI) results in a code conversion error rate (CCER) floor for the scheme. Accordingly, the label switching capacity, i. e., the maximum number of supportable code channels per wavelength, is determined by the acceptable CCER floor. Inter-channel crosstalks due to the finite crosstalk suppression ratio of the optical space switch, and the residual intensity of the sidelobes from the decoder due to the limited on/off ratio of the threshold device are also analyzed, and their impacts on cascadability are manifested by closed-from expressions. By the criteria of 1-dB power-penalty and 5% residue intensity, our numerical simulations show that the network can support up to 20 consecutive nodes for 64-label (8-wavelength, 8-code) switch fabric with 45-dB crosstalk suppression.

Chapter 5: Conclusion

This chapter summarizes the thesis and points out possible future work.

1.3 Reference

[1] C. A. Brackett, " Dense wavelength division multiplexing networks: Principles and applications," IEEE J. Select. Areas Commun., Vol. 8, pp. 948-964, Aug. 1990.

[2] Green, P.E., Jr.; Coldren, L.A.; Johnson, K.M.; Lewis, J.G.; Miller, C.M.; Morrison, J.F.; Olshansky, R.; Ramaswami, R.; Smithand, E.H., Jr. "All-optical packet-switched metropolitan-area network proposal", IEEE/LEOS Journal of Lightwave Technology, Volume: 11 5, May-June 1993, pp. 754 -763.

[3] Norte, D.; Willner, A.E., "All-optical data format conversions and reconversions between the wavelength and time domains for dynamically reconfigurable WDM networks", IEEE/LEOS Journal of Lightwave Technology, Volume: 14 6, June 1996 pp. 1170 –1182.

[4] K. Kitayama, " Code Division Multiplexing Lightwave Networks Based upon Optical Code Converter", IEEE Journal of Selected Areas in Communications, Vol. 16, No. 7, pp. 1309-1319,September 1998.

[5] Daniel J. Blumenthal, Paul R. Prucnal and Jon R. Sauer, "Photonic Packet Switches: Architectures and Experimental Implementations," Proceedings of the IEEE, Vol. 82, No. 11, November 1994, pp.1650-1667.

[6] Amaury Jourdan, et al, " The Perspective of Optical Packet Switching in IP-Dominant Backbone and Metropolitan Networks", IEEE Communication Magazine, Vol. 39, NO. 3, pp. 136-141, March 2001

[7] Gee-Kung Chang, et al, "Low Latency Packet Forwarding in IP over WDM Networks Using Optical Label Switching Techniques, OFC'99, paper MB1, San Diego, CA, USA.

[8] A. Viswanathan, et al, " Evolution of multiprotocol label switching", IEEE Communication Magazine, Vol. 36, May 1998, pp. 165-173.

[9] Banerjee, A., et al "Generalized multiprotocol label switching: an overview of routing and management enhancements", IEEE Communications Magazine, Vol. 39 No. 1, pp. 144 –150, Jan. 2001.

[10] K. Kitayama and N. Wada, "Photonic IP Routing", IEEE Photonic Technology Letters, Vol, 11, pp. 1689-1691, 1999.

Chapter 1

Introduction

1.1 Multi-Protocol Label Switching (MPLS) Technology

The continuous explosive growth in Internet traffic has triggered a surge in bandwidth requirement, both in long haul network and in metro/access network. With the huge capacity of optical fiber, emerging wavelength-division-multiplexing (WDM) technology can meet this bandwidth requirement. Proposed as a means to dramatically increase the transmission capacity in a single fiber originally, WDM network designs have been evolved to include other desirable features, such as, protocol transparency, dynamic reconfigurability, and improved survivability [1-5,10], outperforming the traditional SDH/SONET networks.

Meanwhile, there are several major trends in designing a robot WDM network. These are: (1) Dynamic bandwidth/wavelength provisioning ; (2) Interoperability between vendors/service providers; (3) Intelligent optical routing/signaling; (4) Rings to mesh architecture; (5) Ultra long distance transmission line and (6) collapse of protocol stack. Among them, the most important is that emerging WDM networks need to support intelligent optical routing and switching. For this purpose, efficient routing can be achieved by collapsing of the protocol stacks [6].

As shown figure 1.1(a), traditionally, network designers incorporate several standard layers (IP over ATM over SONET/SDH over Optical) to implement optical systems. Collapse of these layers can enhance WDM network to provide protocol transparency, dynamic recofigurability and improved survivability. In Figure 1.1, two alternative approaches based on multi-protocol label switching (MPLS) technology are proposed for the collapse of protocol stacks.

Figure 1.1(b) shows the layer stack of the first one using the combination of IP and MPLS over optical layer. The combination of IP and MPLS over optical layer promises interoperability and End-to-End QoS, and the optical layer provides high

capacity transport, reliable transport and bandwidth management. Based on current technology, routers based on Internet Protocol/multi-protocol label switching (IP/MPLS) are now reaching capacities in the sub-terabit-per-second throughput range, with 10 Gb/s line cards. To reach multi-terabits-per-second throughputs, massive parallelism and complex interconnection are proposed. Although probably feasible in the medium term as claimed by several vendors for a third generation of router [6], they are not likely to drive the cost down significantly. However, this approach has the advantage of being completely IP-driven, and therefore obviously compatible with traffic engineering and distributed management techniques developed for IP networks.

The other approach shown in Figure 1.1(c) incorporates MPLS in optical layer, and provides OMPLS interface for upper layer, such as, IP layer. For this approach, the optical layer can be partitioned into two basic components: (1) optical switches for direct cross-connection of optical channels without electrical demultiplexing, and (2) MPLS-based control plane, for enhanced management flexibility. This scheme has great potential as it makes simplified forwarding and all-optical label swapping possible. Moreover, application of OMPLS techniques, which allows transport of IP over service-sensitive lower-layer technologies and switching of MPLS on top of optical crossconnects for dynamic resource allocation, provides some flexibility and agility in the redistribution of resources along the network. Thus, it performs better in coping with the massive traffic pattern variations that core networks experience over long periods of time.

To accommodate data traffic in WDM packet-based network, slim protocol stacks with flexible bandwidth-on-demand and dynamic reconfigurability features are designed [7]. In these designs, the second approach (optical multi-protocol label switching (OMPLS) technique) is employed to allow efficient packet forwarding while decoupling the packet routing and forwarding operations to support multiple-routing services [8]. OMPLS also extends beyond the traditional IP forwarding function, and has many advantages including simplified forwarding, efficient explicit

routing, traffic engineering and QoS routing. Most likely, OMPLS will be used as a unifying network management and traffic engineering protocol for a variety of transport systems, thus also extended as Generalized Multi-Protocol Label Switching (GMPLS) [9].

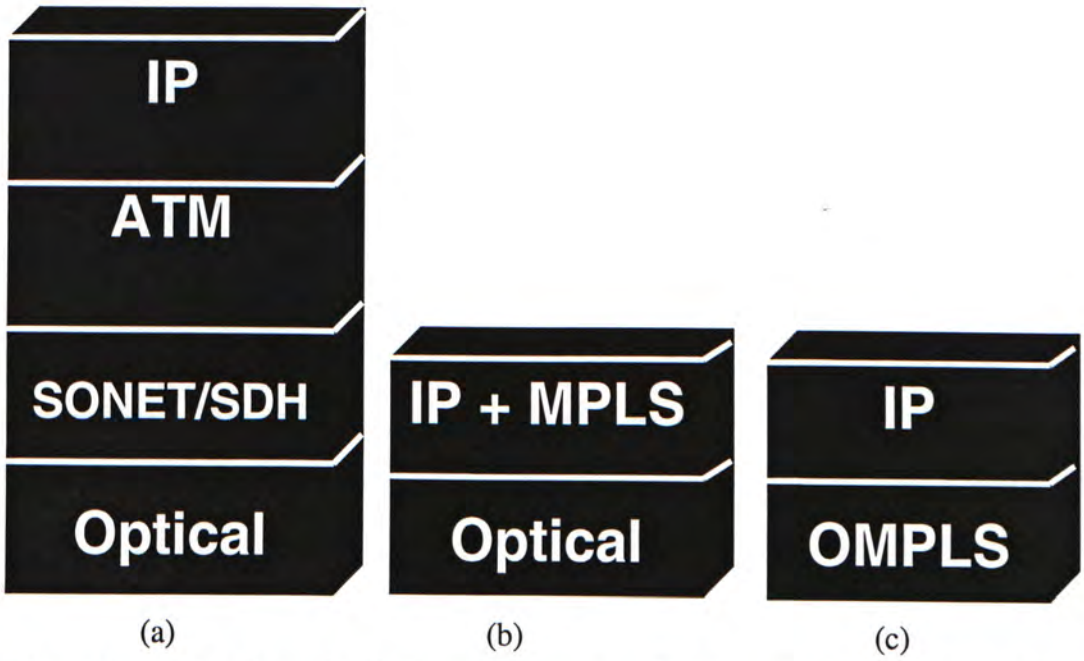

Figure 1.1 Protocol stack solutions for transport of IP-over-WDM networks. (a) Traditional approach, (b) IP/MPLS approach, and (c) IP over OMPLS approach.

1.2 Objective of this Thesis

The architecture issues and the scalability of optical multiprotocol label switching (OMPLS) networks using optical orthogonal codes (OOC) as labels are investigated in this thesis. The thesis is organized as follows.

Chapter 1: Introduction

This chapter describes some network trends that meet the rapid growth of the bandwidth requirement. The promising trend is the collapse of stacks. There are two approaches to incorporate optical layer and MPLS into WDM networks for intelligent optical routing/signaling: IP/MPLS and IP-over-OMPLS.

Chapter 2: Optical MPLS Network and Optical Label Schemes

This chapter describes a generic photonic MPLS network and its layer infrastructure. With this infrastructure, an overview of four primary optical MPLS technologies is given in this chapter. These are (1) time-division label scheme, (2) wavelength-division label scheme, (3) frequency-division label scheme and (4) code-division label scheme.

Chapter 3: Architecture of OOC-based OMPLS network

The architecture issues of the generic OOC OMPLS network are described in this chapter. First, the fundamental idea of OOC OMPLS is given. Then, we will focus on the most important component of this network, a four-stage code converter for core router. Finally, the various implementations of every individual stage of the code converter are outlined and compared. There are encoders/decoders, threshold device and optical space switch fabric.

Chapter 4: Scalability of OOC-based OMPLS network

The fundamental limits on the scalability of optical multi-protocol label switching (OMPLS) networks using optical orthogonal codes (OOC) as labels are investigated in this chapter. Based on the proposed four-stage architecture of the optical core router, closed-form results for the label switching capacity and the network

cascadability are derived. Originated from the intrinsic uni-polar property of OOC, the multi-access interference (MAI) results in a code conversion error rate (CCER) floor for the scheme. Accordingly, the label switching capacity, i. e., the maximum number of supportable code channels per wavelength, is determined by the acceptable CCER floor. Inter-channel crosstalks due to the finite crosstalk suppression ratio of the optical space switch, and the residual intensity of the sidelobes from the decoder due to the limited on/off ratio of the threshold device are also analyzed, and their impacts on cascadability are manifested by closed-from expressions. By the criteria of 1-dB power-penalty and 5% residue intensity, our numerical simulations show that the network can support up to 20 consecutive nodes for 64-label (8-wavelength, 8-code) switch fabric with 45-dB crosstalk suppression.

Chapter 5: Conclusion

This chapter summarizes the thesis and points out possible future work.

1.3 Reference

[1] C. A. Brackett, " Dense wavelength division multiplexing networks: Principles and applications," IEEE J. Select. Areas Commun., Vol. 8, pp. 948-964, Aug. 1990.

[2] Green, P.E., Jr.; Coldren, L.A.; Johnson, K.M.; Lewis, J.G.; Miller, C.M.; Morrison, J.F.; Olshansky, R.; Ramaswami, R.; Smithand, E.H., Jr. "All-optical packet-switched metropolitan-area network proposal", IEEE/LEOS Journal of Lightwave Technology, Volume: 11 5, May-June 1993, pp. 754 -763.

[3] Norte, D.; Willner, A.E., "All-optical data format conversions and reconversions between the wavelength and time domains for dynamically reconfigurable WDM networks", IEEE/LEOS Journal of Lightwave Technology, Volume: 14 6, June 1996 pp. 1170 –1182.

[4] K. Kitayama, " Code Division Multiplexing Lightwave Networks Based upon Optical Code Converter", IEEE Journal of Selected Areas in Communications, Vol. 16, No. 7, pp. 1309-1319,September 1998.

[5] Daniel J. Blumenthal, Paul R. Prucnal and Jon R. Sauer, "Photonic Packet Switches: Architectures and Experimental Implementations," Proceedings of the IEEE, Vol. 82, No. 11, November 1994, pp.1650-1667.

[6] Amaury Jourdan, et al, " The Perspective of Optical Packet Switching in IP-Dominant Backbone and Metropolitan Networks", IEEE Communication Magazine, Vol. 39, NO. 3, pp. 136-141, March 2001

[7] Gee-Kung Chang, et al, "Low Latency Packet Forwarding in IP over WDM Networks Using Optical Label Switching Techniques, OFC'99, paper MB1, San Diego, CA, USA.

[8] A. Viswanathan, et al, " Evolution of multiprotocol label switching", IEEE Communication Magazine, Vol. 36, May 1998, pp. 165-173.

[9] Banerjee, A., et al "Generalized multiprotocol label switching: an overview of routing and management enhancements", IEEE Communications Magazine, Vol. 39 No. 1, pp. 144 –150, Jan. 2001.

[10] K. Kitayama and N. Wada, "Photonic IP Routing", IEEE Photonic Technology Letters, Vol, 11, pp. 1689-1691, 1999.

Chapter 2

Optical MPLS Network and Optical Label Schemes

2.1 Optical MPLS Network

A generic optical MPLS network is shown in Figure 2.1. The source node A generates IP packets, which are routed by conventional electronic routers (i.e. IP routers) to an edge device (the ingress router) of the optical MPLS network. Labels are encapsulated onto IP packets at the optical edge device located at the ingress router. The optical core routers perform routing and forwarding by label swapping. When packets leave the photonic MPLS network at another edge device (the egress router), the egress router removes the labels and forwards the packets to its destination.

Figure 2.2 shows the operation of network elements in the layer infrastructure of the OMPLS network [1]. IP packets are generated at the electronic routing layer (IP routers) and processed in an OMPLS adaptation layer that encapsulates IP packets with an optical label without modifying the original packet structure. The adaptation layer also converts the packet and label to a new wavelength specified by local routing tables. An optical multiplexing layer multiplexes labeled packets onto a shared fiber medium. Several optical multiplexing approaches may be used including insertion directly onto an available WDM channel [2], packet compression through optical time multiplexing or time interleaving through optical time division multiplexing [3], and optical code-division multiplexing [4]. In the optical MPLS network, core routers, which can be partitioned into two basic parts: control component and forwarding component, perform routing and forwarding functions. In the control component, the routing algorithm computes a new label and wavelength from an internal routing table giving the current label and optical interface (including current wavelength and fiber port). The routing tables (at egress and core routers) are generated by mapping IP addresses into smaller pairs of labels and wavelengths and

distributing them across the network via piggyback on top of routing protocols (e.g. OSPF or PIM) or a separate protocol (e.g. Label Distribution Protocol)[5]. The forwarding component has the responsibility of swapping the original label with the new label and physically converting the labeled packet to the new wavelength. The reverse process of optical demultiplexing, adaptation and electronic routing are performed at the egress node.

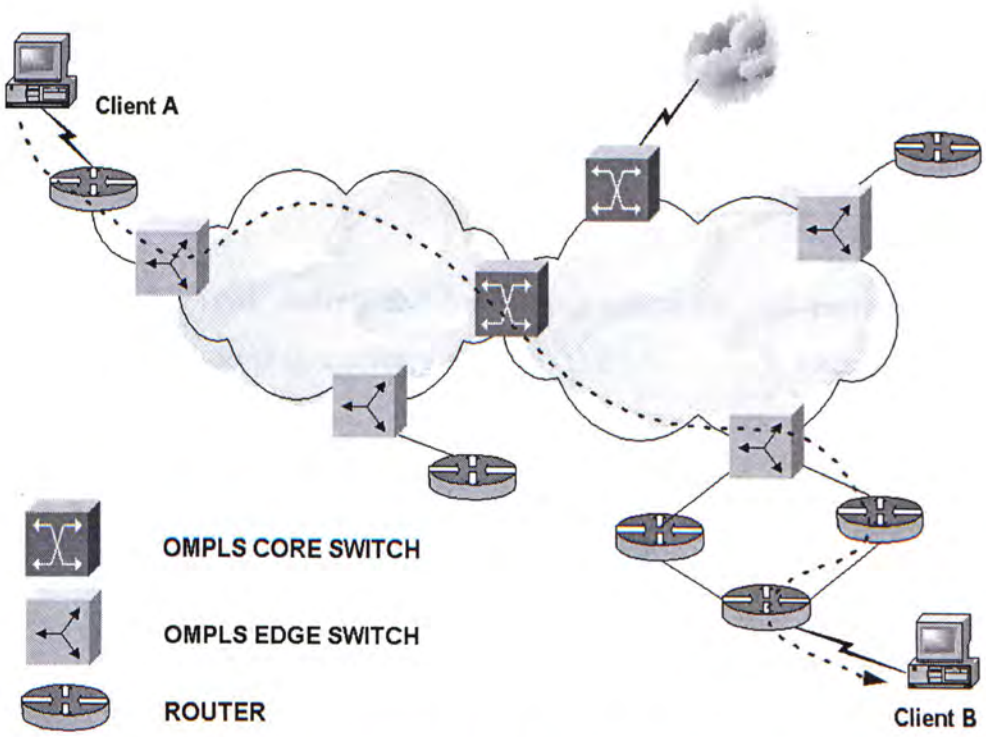

Figure 2.1 A generic Optical Multi-Protocol Label Switching (OMPLS) network. The dash line shows the label switched path (LSP) that routes IP packets from the source, through router, edge switch and core switch, to the destination.

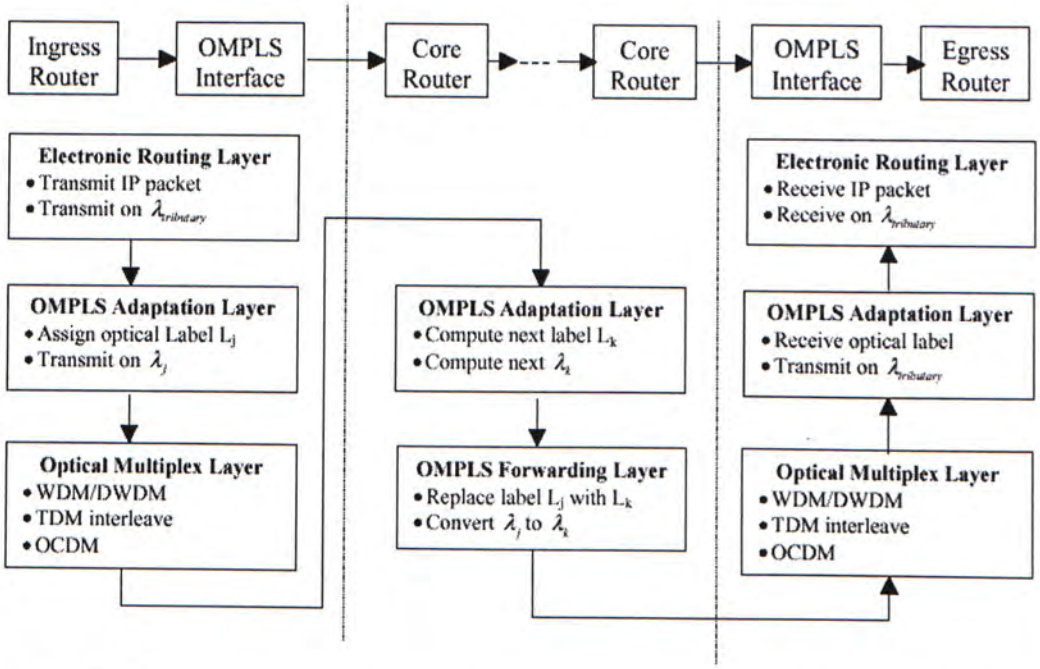

Figure 2.2 Layered routing and forwarding hierarchy and associated network element connection diagram for a generic OMPLS network. (Adapted From Ref [1])

2.2 Optical Label Schemes

As shown in Figure 2.3, the label embedded in the IP packet could be implemented by (a) time slot, (b) wavelength, (c) subcarrier or (d) code, and usually denotes critical label-switched-path information such as the source and destination. For optimum performance:

1. Optical label should not deprive much wavelength resources originally dedicated for data channel;
2. Optical label swapping should be easily implemented, preferably in optical domain;
3. Optical label should be immune to the accumulated distortions from dispersion, timing jitter, and interference from other co-propagation labels.

Based on these criteria, there are four primary optical label schemes proposed previously. As shown in Figure 2.3, there are (1) time-division label scheme, (2) wavelength-division label scheme, (3) frequency-division label scheme and (4) code-division label scheme.

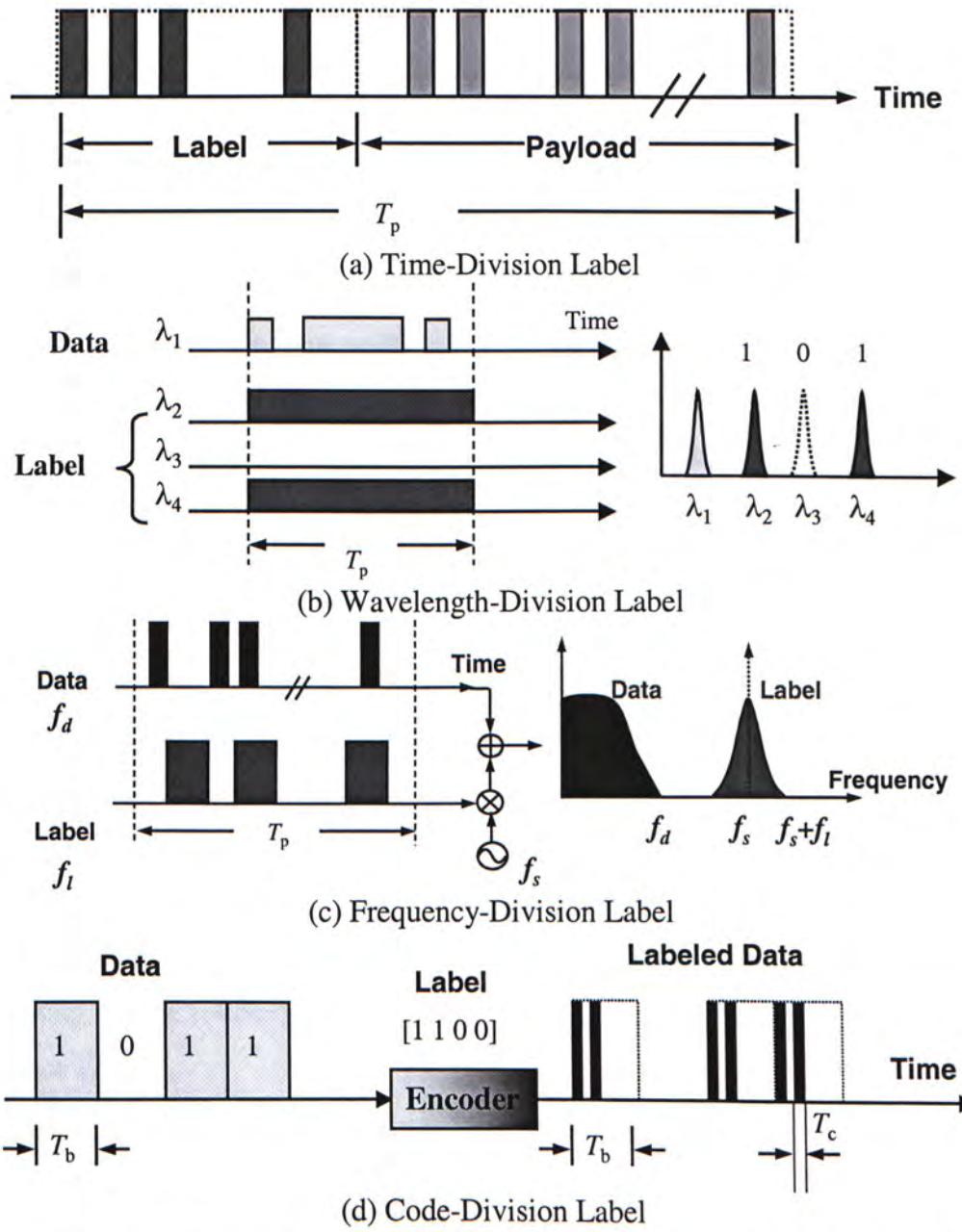

Figure 2.3 The schemes of optical label technology: (a) Time-division Label, (b) Wavelength-division label, (c) frequency-division label and (d) Code-division label. T_p is the packet duration; λ_1 is the carrier of data, $[\lambda_2, \lambda_3, \lambda_4]$ are for label, different combinations of these carriers denote different labels; f_d and f_l are the rate of data and label, f_s is the subcarrier frequency; T_b and T_c are the duration of data bit and code chip.

2.2.1 Time-division OMPLS scheme

Figure 2.3(a) shows a schematic diagram of time-division OMPLS scheme. In this label scheme, optical label is implemented by adding a routing header before the payload in time domain. The bit rate of routing header is usually the same as or lower than the data rate [6]. The former one avoids much buffering time for label processing, but puts some challenges on the processing capacity of label processor. Since the label rate is the same as the data rate, for the current transport networks, the label processor must work at multi-Gbps rate to process label recovery, label swapping and packet forwarding. The latter one processes label in a comparably lower rate, but needs more buffering time for the fixed number of optical label bits. Due to the mature electronics technologies (e.g. FPGA and ASIC) in lower processing rate, this approach is preferable at current stage.

All-optical label processing (recovery, swapping and reinserting) is essentially important for OMPLS networks. For time-division label scheme, traditional header processor could be introduced for label processing. However, with the coherent nature of optical routing label, label swapping can be realized by optical label conversion with simple XOR gate [7]. Its operation principle is simple, just using another sequence (swapping sequence) to change the old label via optical XOR processing. In the following, its operational experiment was described according to reference [7][1].

Figure 2.4 shows a schematic diagram of the label-swapping scheme with the interferometric XOR gate. At the input of the core switch, the optical signal in incoming packets is split into two copies. One copy is forwarded to the switch control component to perform label discovery and header clock recovery, both necessary for any header modifications. In the control component, the swapping sequence is located in the routing table according to the received old label and optical interface. Then, the optical swapping sequence, modulated onto CW-light at a

[1] To avoid redundant reference indication, we do not put quota number while presenting the experimental setup and results.

fixed internal wavelength λ_{int}, is coupled into one of the interferometer arms (port #2), while the other copy of input packet at λ_{in} is coupled into the other. Meanwhile, CW-light at the desired output wavelength, λ_{out}, is coupled into port #3. Due to cross-phase modulation (XPM), the output packet at λ_{out} corresponds to the logic XOR of the input packet and the swapping sequence, i.e., a ZERO bit in the swapping sequence will leave the input data bit unchanged at the output, while a ONE bit will reverse the bit of the input packet. One advantage of the scheme is that it has no restriction on the payload data rate, since the time-slot corresponding to the payload is kept to be ZERO bit, thus no effect on the original data payload. Furthermore, 40-Gbit/s wavelength conversion has previously been performed in a wavelength converter, indicating the high-speed potential of the scheme [7].

The experimental set-up implemented in [7] is shown in Figure 2.5, which is used to investigate the XOR label-swapping scheme at 10 Gbit/s. In order to generate the input packet sequence and the label swapping sequence economically, a 10-Gbit/s RZ data signal containing the input packet sequence in tandem with a label swapping sequence (Δ) is generated at 1538 nm. As shown in Figure 2.5, the signal is passively split into two copies. After delaying one copy appropriately with respect to the other, the swapping sequence is fed into one arm of the Michelson Interferometer (MI), while the packet header is fed into the other arm. Meanwhile, another 1543 nm CW-light source is coupled into the MI at port #3. Output from port #3 is the wavelength converted output packet sequence (including untouched data payload and swapped packet header). Finally, a BPF filter is used to selects the output packet sequence for detection and error counting.

Experimental results (the measured input and output packet sequences) are shown in Figure 2.6. The packet has a packet length of 123 bits, including a 23-bit header, a 7-bit guard band and a 93-bit payload. As expected, the input and output packet sequences are identical in data payload, except that the bits in the header have been altered by the label-swapping processing. In Figure 2.7, the input header and partial

payload along with the corresponding label swapping sequence and output header are enlarged to verify the label-swapping processing. As shown in the output packet, the old header has been changed to the new header by XOR processing with the swapping sequence.

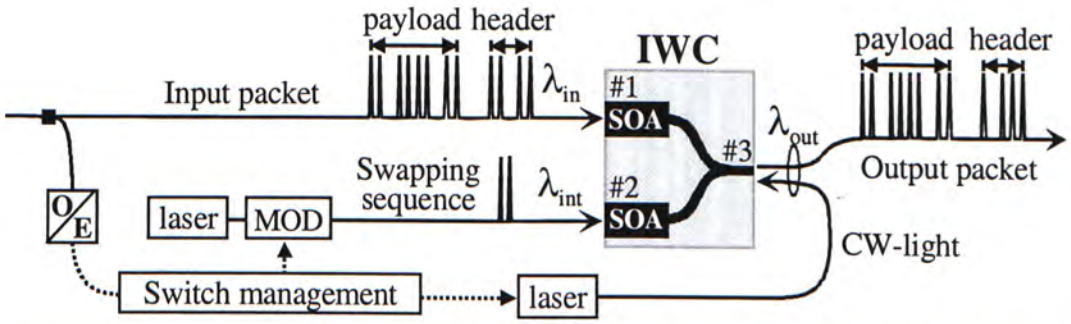

Figure 2.4 Schematic of practical implementation of label swapping scheme. MOD: modulator. (Adapted from Ref [7])

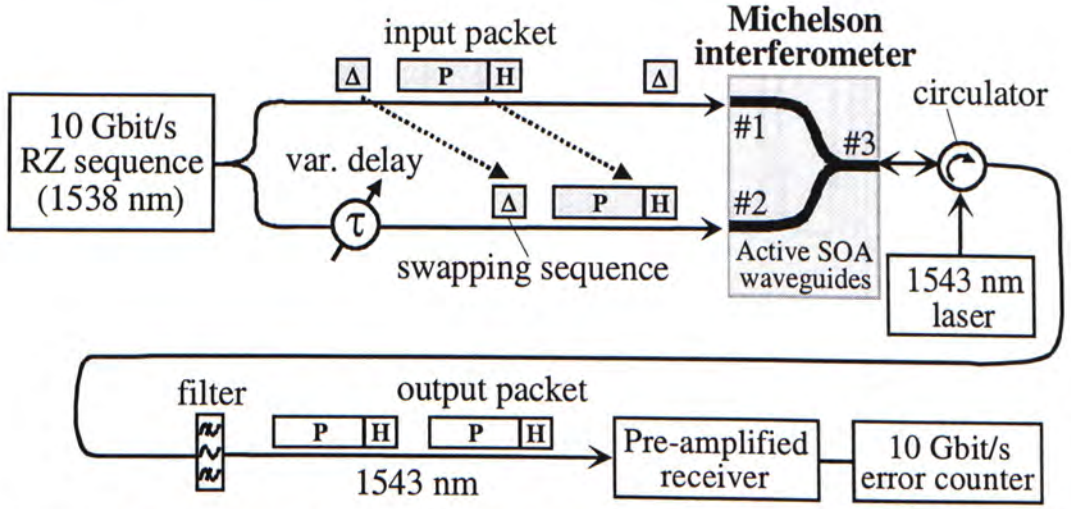

Figure 2.5 Experimental set-up for time-division label swapping. (Adapted from Ref [7])

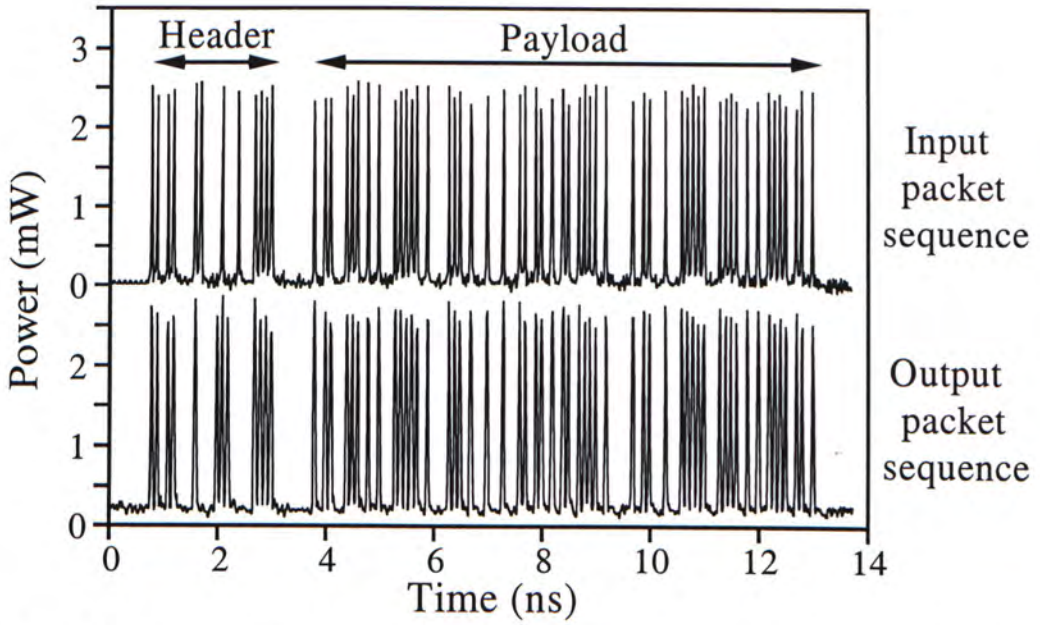

Figure 2.6 Measured input and output packet sequences. (Adapted from Ref [7])

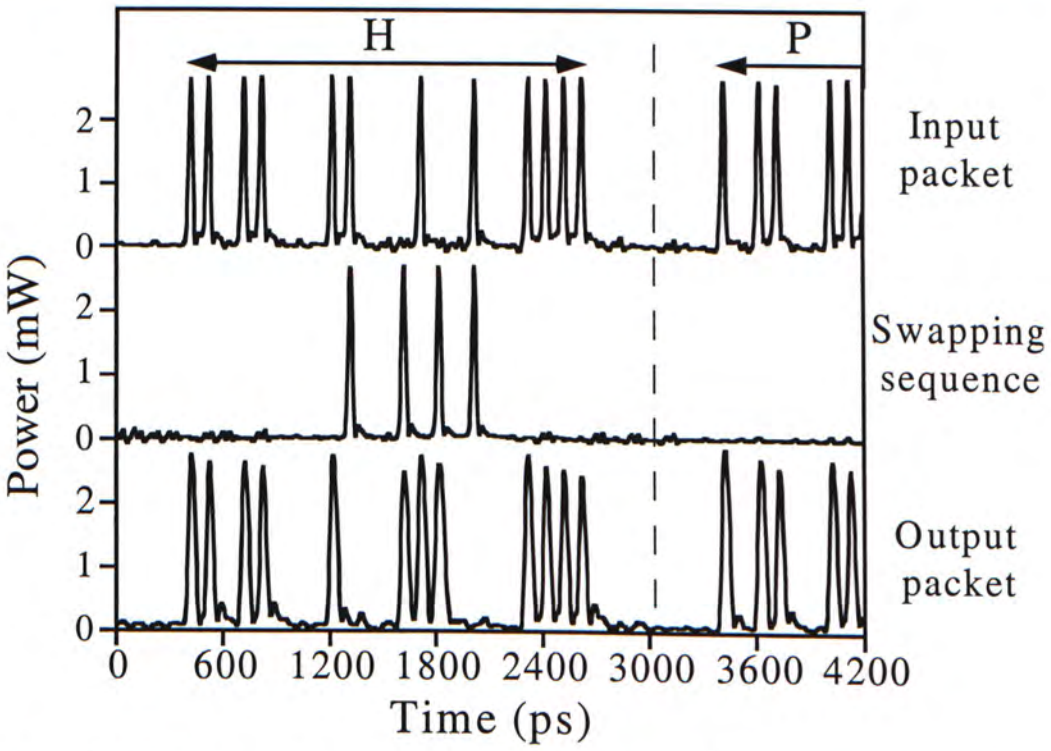

Figure 2.7 Scheme verification-enlargement of header (H) and payload (P).
(Adapted from Ref [7])

2.2.2 Wavelength-division OMPLS scheme

Wavelength-division optical label is also called wavelength-coded label. Shown in Figure 2.3(b), three public wavelengths (λ_2, λ_3 and λ_4) are reserved for label coding, and data payload is carried on its lightwave carrier (λ_1). Different combinations of present or absence of these three public wavelengths represent different destination labels. In figure 2.3(b), λ_2 and λ_4 are present, λ_3 is absent, thus the coded wavelength label is [1 0 1]. For an *N*-public-wavelength label system, the total number of wavelength labels is 2^N. Therefore, though *N* wavelengths are reserved only for label coding, this number is small compared with the supportable data channels (2^N).

For a wavelength-division OMPLS network, the all-optical label switching router (core router) is easier to implement compared with other OMPLS schemes, since it can be implemented with FBG. One representative system based on wavelength-division OMPLS network was proposed by Wada and Harai [8][2], though their proposal has very low wavelength efficiency. As shown in Figure 2.8, the header carries a wavelength-coded label that corresponds to a destination node. In the scheme, multi-wavelength labels are carried on λ_{1A}, λ_{1B}, λ_{1C}, and λ_{1D}. Payload data uses another different wavelength (λ_{1E}). Wavelengths ranging from λ_{1A} through λ_{1E} are defined as a wavelength band $\lambda_{1A\text{-}E}$.

The multi-wavelength label switching router [8] is proposed in Figure 2.9. The infrastructure consists of two basic subsystems: the control components (*M* λ-label processor) and the forwarding components (label/data separator, 1x*N* optical switch and label changer,). At first, the separator separates packet label and burst data. Then in the control components, optical label recognition is performed in parallel manner by *M* λ-label processor. Using the label information, the *M* λ-label processor configures the forwarding components. Therefore, the IP packet can be transported to a desitnated port though the1x*N* optical switch. Meanwhile, according to the new

[2] To avoid redundant reference indication, we do not put quota number while presenting the experimental setup and results.

label provided by the control component, the label changer can generate a new label for the output packet.

Figure 2.10 shows the experimental setup [8], which can be partitioned into three sections: *M* λ-packet transmitter, 33-km dispersion shifted fiber (DSF), and 3-port *M* λ-LSR.

In the optical packet transmitter, the supercontinuum (SC) light source with bandwidth over 140 nm is generated and split into two copies for header insertion and data modulation with $LiNbO_3$ intensity modulators (IM). For header insertion, *M* λ-pulse from SC source is disassembled into three pulses by the three-section FBG to form the *M* λ-label ("λ_{1A}, λ_{1C}, λ_{1B}" in Figure 2.10). For data modulation, optical pulse at wavelength λ_{1E} is extracted by a BPF at first, and 64bit-long burst data is modulated on the optical carrier. After optical coupler, optical packet with three-chip *M* λ-label and data is all-optically generated.

In the *M* λ-LSR, the label and data is separated by an optical BPF. The data signal is forwarded to the 1x3 optical switch, while the label signal is forwarded to the optical correlator array for label processing. In the label processor, three FBGs are used as optical correlators. If the input wavelength label is matched with the setting of an FBG correlator, the output takes a high value corresponding to the autocorrelation peak, and the correlation signal is converted to the electrical domain, and amplified to open the IM gate switch. Thus, the packet can be transported to an objective output port. Otherwise, for unmatched case, the correlated signal takes a low value corresponding to the crosscorrelation. Therefore, the bias of the IM gate is not changed, and then the gate switch keeps close. The label processor can be configured to open a specific switch and direct the matched packet to the destination port.

Experimental results are shown in Figure 2.11. Figure 2.11(a) and (b) shows the generated *M* λ –label (λ_{1A}, λ_{1C}, λ_{1B}) and the packet, respectively. When the input label is (λ_{1A}, λ_{1C}, λ_{1B}), the correlation outputs of FBG1* with the setting of (λ_{1B}, λ_{1C}, λ_{1A}) and

FBG3* with the setting of (λ_{1C}, λ_{1B}, λ_{1A}) are shown in Figure 2.11(c) and (d). For the matched case (Figure 2.11(c)), correlation signal has a high autocorrelation peak; while for unmatched case (Figure 2.11(d)), the signal has no high peak. This is the experimental demonstration of the all-optical M λ-label discovery. Figure 2.11(e) and (f) shows the measured payload data at Ports 1, 2, and 3, corresponding to the two different input packets having label of (λ_{1A}, λ_{1C}, λ_{1B}) matched with FBG1* and (λ_{1A}, λ_{1B}, λ_{1C}) matched with FBG3*. It demonstrated that the M λ-LSR could switch optical path, which depends on the input wavelength label and optical interface.

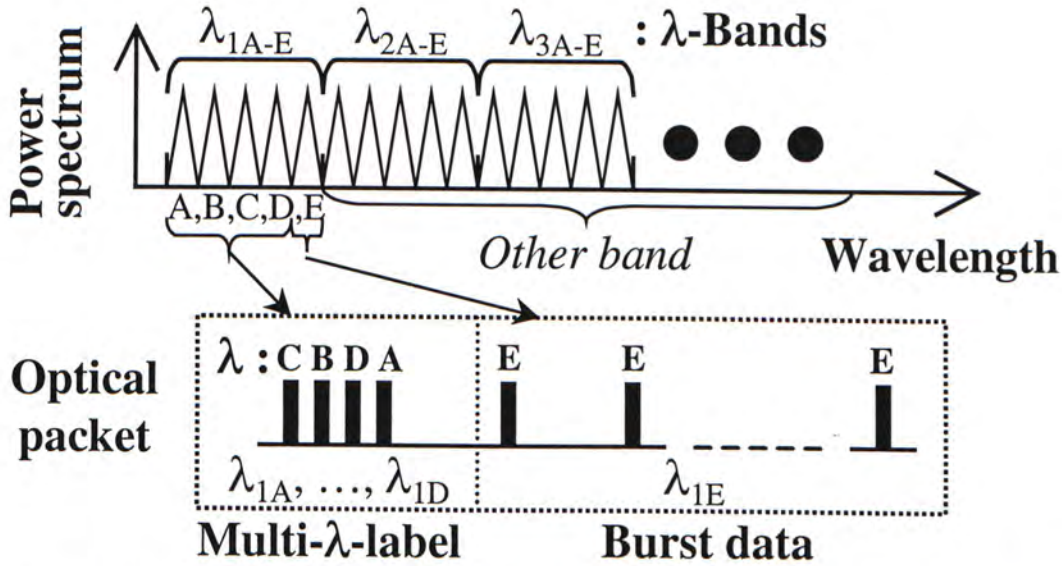

Figure 2.8 Schematic diagram of packet format for multi-wavelength label switching scheme. (Adapted from Ref [8])

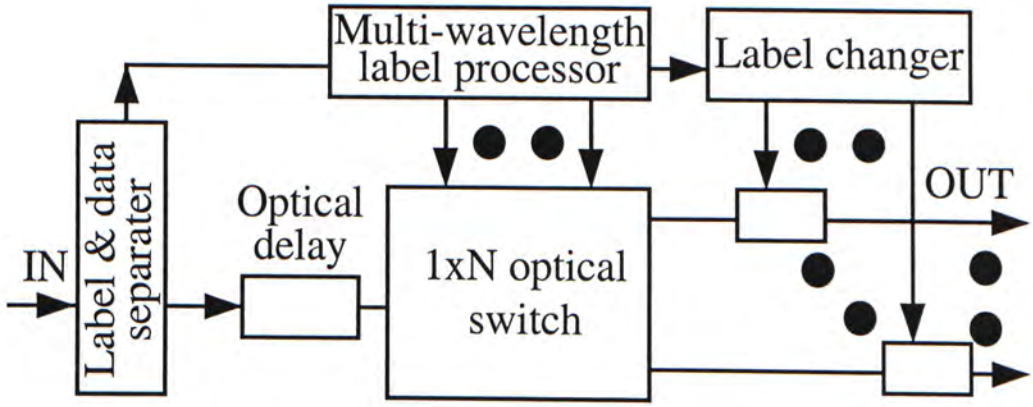

Figure 2.9 Multi-wavelength label switch router. (Adapted from Ref [8])

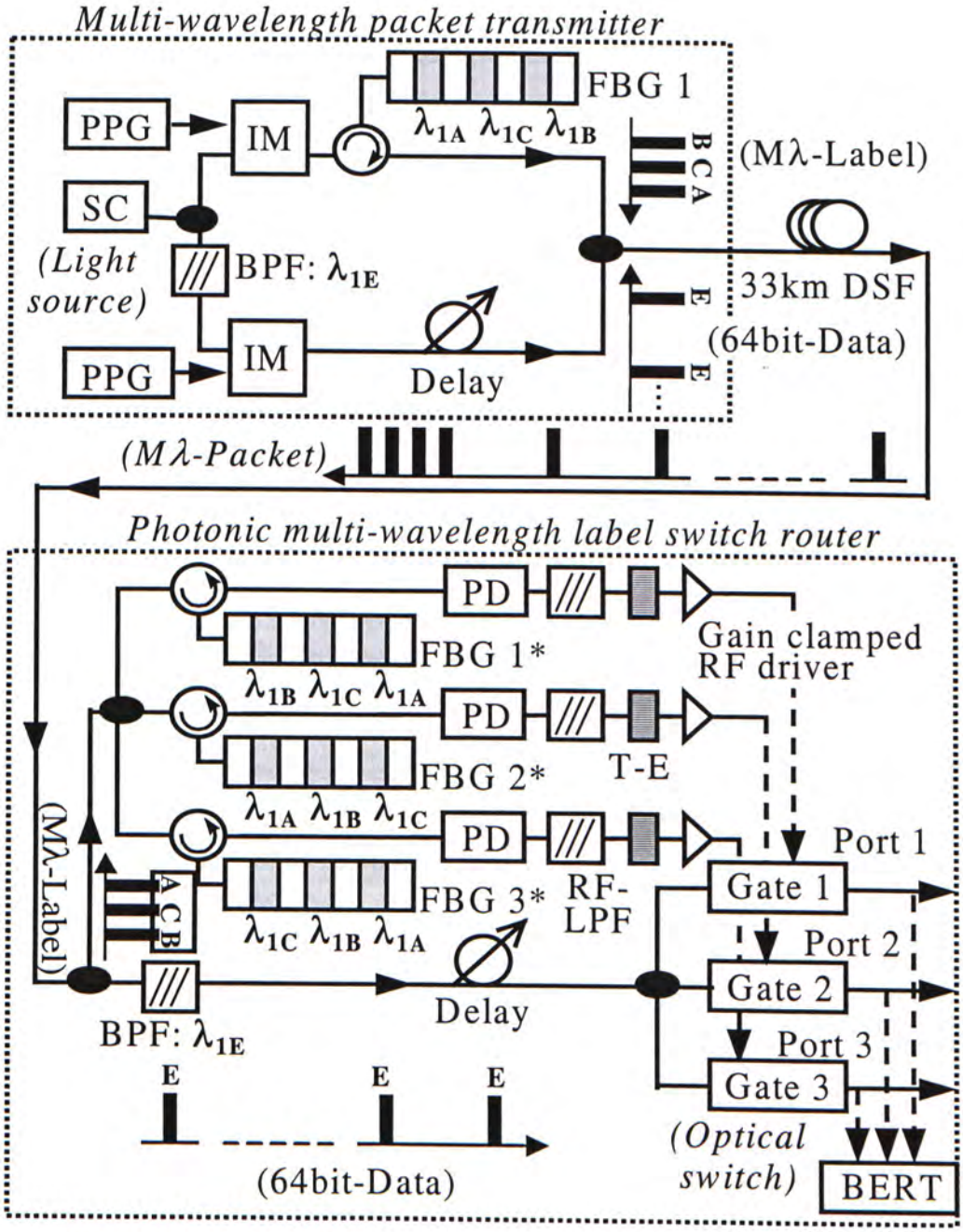

Figure 2.10 Experimental setup of multi-wavelength label switching router. (Adapted from Ref [8])

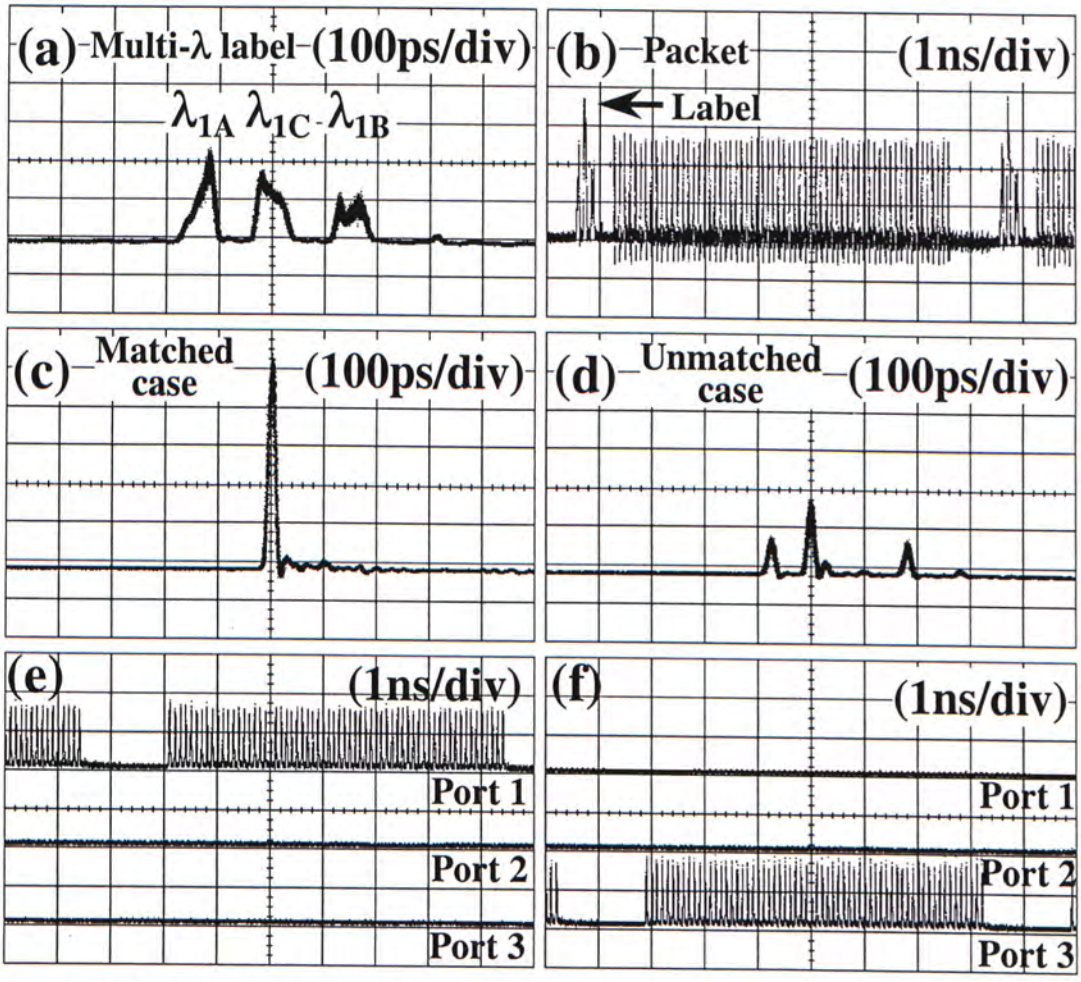

Figure 2.11 Experimental results of multi-wavelength label switching. (Adapted from Ref [8])

2.2.3 Frequency-division OMPLS scheme

Figure 2.3(c) shows the operational principle of the frequency-division optical label scheme. In this scheme, optical label is carried by out-of-band subcarrier [6]. The payload and label are transmitted at different rates, and label recovery is performed independent of the payload data rate by using simple microwave filtering techniques. Subcarrier label recovery is performed using optical and microwave amplitude detection alleviating the need for RF coherent techniques and phase synchronization across the network. Furthermore, the mature electronics guarantees the practicability of optical subcarrier label scheme. Thus, there are more and more attention paid to this kind of label implementation and testbed [9-11].

Another attraction of frequency-division optical label is packet transparency. In this scheme, packet transparency is realized by setting a fixed label bit rate and modulation format independent of the packet bit rate. The choice of label bit rate is determined by various factors including the speed of the burst-mode label recovery electronics and the duration of the label relative to the shortest packets at the fastest packet bit rates, etc. Additionally, running the label at a lower bit rate allows the use of lower cost electronics to process the label. The label and packet bits can be encoded using different data formats to facilitate data and clock recovery.

However, subcarrier label system limits the payload bit rate. In order to avoid the label's interference to the payload, there must be some guard-band between the payload spectrum and subcarrier spectrum. For example, if the subcarrier frequency is 10 GHz and label format is 100-Mbps NRZ, the payload rate should be below 9 Gbps to avoid the leakage of label spectrum.

With both pros and cons, optical subcarrier label is the most promising candidate for OMPLS network. Therefore, all-optical label swapping for this scheme gains much attention both in academic and commercial institutes. Currently, researchers prefer to use remove-and-reinsert mode label swapping for subcarrier label scheme. In essence, it is a three-stage label processing. At the first stage, subcarrier label is

extracted and removed in all-optical ways. At the second stage, label is recovered and label information is fed to the control plane to determine the next label. Finally, at the final stage, the new label is remodulated at the same microwave carrier frequency for the IP packets. Currently, there are three major research projects on this scheme [9-11].

2.2.3.1 UCSB Testbed

The first project is implemented at the University of California at Santa Barbara (UCSB) [9][3]. The optical subcarrier modulation (OSCM) label technique is shown in Figure 2.12. A differentially modulated interferometric modulator is used to combine baseband payload and subcarrier label onto an optical carrier. The RF power spectrum of the packet is also shown in Figure 2.12.

For label swapping, a two-stage label processor with two wavelength converters is proposed in Figure 2.13. Besides the desire subcarrier label swapping function, this processor also provides independent wavelength conversion, thus enhancing the flexibility of the scheme.

The first XGM-SOA-WC performs three functions including (1) conversion to an internal wavelength, (2) suppressing of the SCM label, and (3) reduction in modulation dynamic range. Conversion to an internal wavelength allows the use of a fixed frequency optical filter to separate unconverted and converted signals. A side effect of this wavelength conversion is bit inversion, which can be negated in the second wavelength converter. While the payload is converted to a new wavelength via XGM, the label is suppressed due to the low pass filter characteristics of the SOA-WC. Reduction in output dynamic range of the first converter sets a stable operating point for the XPM interferometric SOA-WC.

The second XPM SOA-WC takes the responsibility that the throughgoing payload and a new label are reinserted onto the new wavelength. The XPM SOA-WC is

[3] To avoid redundant reference indication, we do not put quota number while presenting the experimental setup and results.

operated in the inverting mode to negate bit inversion of the baseband in the XGM SOA-WC. Square law detection of the subcarrier makes label recovery insensitive to the inversion due to wavelength conversion [9]. The converted payload from the XGM SOA-WC is fed to one arm of the interferometer to add the payload onto a new wavelength optically. Meanwhile, a new SCM label is added onto the converted payload by current modulation of the SOA in the other arm. At the same time, the nonlinear transfer function of the XPM converter enhances the extinction ratio of the outgoing payload. Therefore, a cascadable packet switched node with label swapping capability is realized with optical 2R regeneration of the payload and the swapping of the SCM label.

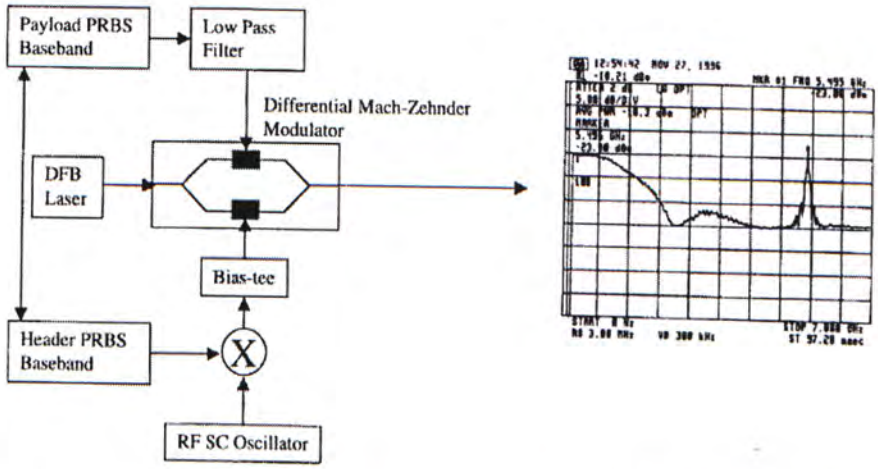

Figure 2.12 Differential interferometric transmitter used to generate packets with payload at baseband and header multiplexed on a subcarrier. Also shown is the resulting RF power spectrum. (Adapted from Ref [9])

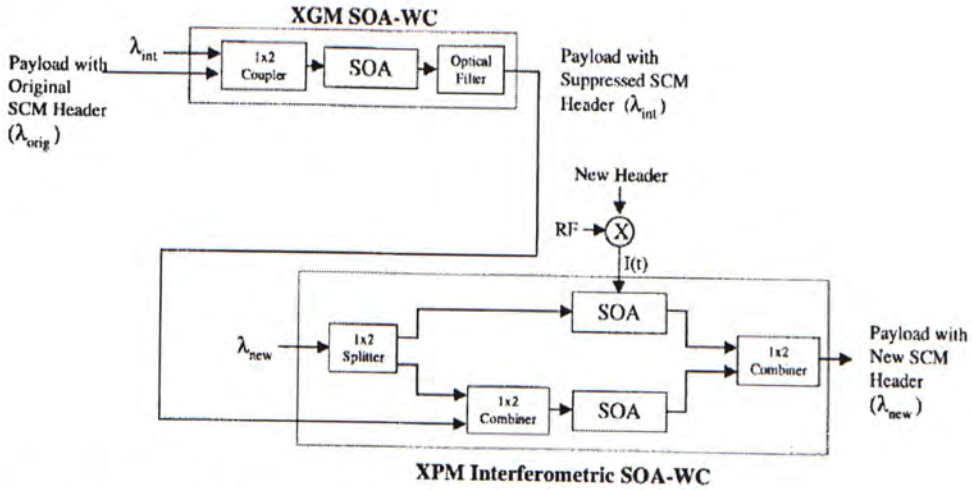

Figure 2. 13 Double stage SOA-based wavelength converter capable of optical header label swapping by subcarrier suppression and replacement. The first stage is based on XGM and the second on XPM interferometric structure. Subcarrier header replacement is performed with electronic modulation of SOA current in one arm of the interferometer. (Adapted from Ref [9])

2.2.3.2 UC-Davis Testbed

The second experimental testbed is reported from the University of California at Davis [10][4]. Figure 2.14 shows the schematic diagram of the experiment. This system represents the core switch of an optical label switching router/node. It consists of an optical-subcarrier transmitter, and optical-header/data separator, a header detector, a forwarding table, a switch controller, a tunable wavelength converter including a tunable laser and semiconductor optical amplifier (SOA), a uniform-loss-cyclic frequency (ULCF) AWG, header rewriters and receivers. The experiment setup works as follows:

Stage I: In the transmitter, the original label (header_1) at 622 Mb/s is modulated on a 14-GHz subcarrier, and then combined with the 2.5-Gb/s data payload packet. After that, the combined RF signal is added onto the optical carrier (1549.3 nm). Therefore, the modulated signal includes double side band subcarrier label appearing 14 GHz away from the center optical wavelength 1549.3 nm.

Stage II: A Fiber Bragg Grating (FBG) with peak reflectivity centered at 1549.3 nm is used as the optical-head/data separator to separate the subcarrier label and data payload. The FBG has higher than 99.9% peak reflectivity and a Half-Width-at-Half-Maximum pass band of 5 GHz. Therefore, the data payload appearing at the center lobe will be nearly perfectly reflected, and the subcarrier label appearing at the double side band will be nearly completely transmitted. Then, the optical circulator separates the input signal, the reflected data payload, and the transmitted subcarrier label.

Stage III: The 40 bit long optical-label is first detected by the header detector, and then compared with the entry of the forwarding table to locate new optical-label, finally the controller generates a switch control signal and new optical-label content. The data payload is delayed via the 50-meter optical fiber for approximately 250 ns optical delay, and fed to the SOA-based wavelength converter. This data payload is

[4] To avoid redundant reference indication, we do not put quota number while presenting the experimental setup and results.

converted to another counter-propagating optical wavelength source, which is generated by the tunable laser. This counter-propagating geometry avoids the need of an optical filter to select the transmitting tunable laser output, and also further reduces leakage of the subcarrier header from the higher modulation frequency to the base-band data payload. Of course, a side effect of wavelength conversion is bit inversion, which could be corrected by cascading another inverting wavelength converter in tandem. The switch control signal from the controller is forwarded to the tunable laser, tuning its wavelength output to the one that corresponds to the desired output destination port of the AWG.

Stage IV: At the output ports of the AWG, an additional optical modulator works as header rewriter to overmodulate a new subcarrier label on the routed data payload, and hence achieving optical-label swapping.

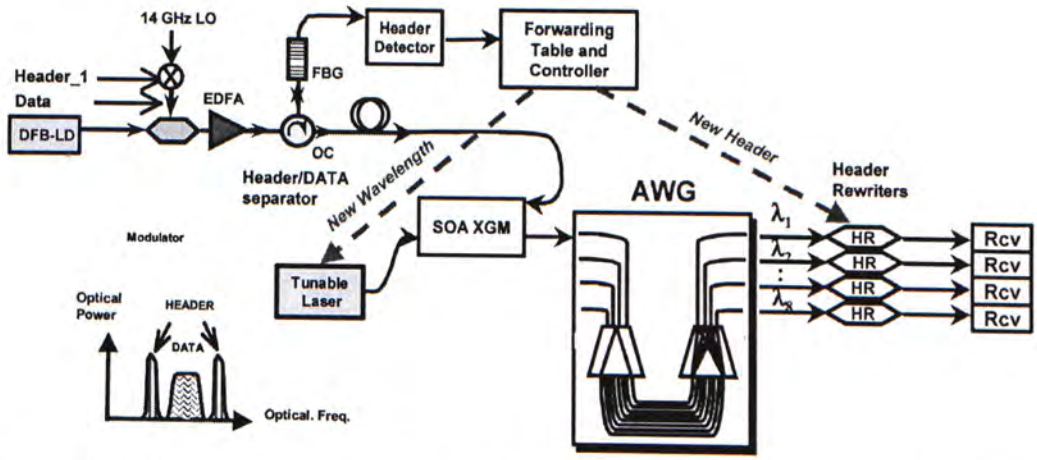

Figure 2.14 Experimental Setup of UC-Davis testbed. (Adapted from Ref [11])

2.2.3.3 NCTU-Telecordia Testbed

The third testbed [11][5] was implemented in the joint project of National Chiao-Tung University and the Telecordia Technologies. In this project, optical single-sideband (OSSB) modulation technique is proposed to implement the optical subcarrier label. In this way, the resultant optical spectrum contains only one subcarrier label sideband, which significantly reduces the interference from the label to the data payload. Another advantage of using OSSB subcarrier label is that it can avoid the fiber dispersion-induced carrier suppression effect [12], which can limit the transmission distance between switching nodes.

The experimental setup for transmitter, intermediate switching node and detector is shown in Figure 2.15.

In the transmitting node, a 50-mW 1551-nm DFB-MQW laser and a two-electrode $LiNbO_3$ external Mach-Zehnder modulator (MZM) with a 3-dB bandwidth of 20 GHz and an insertion loss of 4 dB were used. A bursty 155-Mb/s ASK subcarrier label at 12 GHz was applied to a hybrid coupler whose two outputs have 90^o phase shift with respect to each other. These two outputs were then combined with a bursty 2.5-Gb/s data and data invert, respectively. Two low-pass filters with a 3-dB bandwidth of 2.4 GHz were used to prevent the tails of the 2.5-Gbs NRZ data from interfering with the ASK subcarrier. The two combined NRZ data and ASK subcarrier outputs were then used to drive the two electrodes of the MZM, respectively.

In the switching node, the received optical signal was split into three copies. The first copy was simply fed to a data payload receiver for system monitoring. The second copy was fed to the label receiver for label processing (recovery and swapping). The third copy was reserved for label swapping. This optical signal passes through a Fiber Fabry-Perot (FFP) filter via an optical circulator, so that the old subcarrier label was notched out. The FFP filter has a free spectral range (FSR)

[5] To avoid redundant reference indication, we do not put quota number while presenting the experimental setup and results.

of 1500 GHz, a finesse of 100, and a reflection loss of 1.5dB. The optical signal with its subcarrier label suppressed subsequently passed through a polarization controller and another MZM for label reinsertion. At the MZM, the optical signal was remodulated with a new ASK subcarrier label, which had the same carrier frequency and optical modulation index (OMI) at those of the old subcarrier label. At the output of the switching node, an EDFA with an output power gain of 12dB was used to amplify the optical signal for inter-node transmission.

In the detection node, data payload and subcarrier label are processed in the same way as those in switching node.

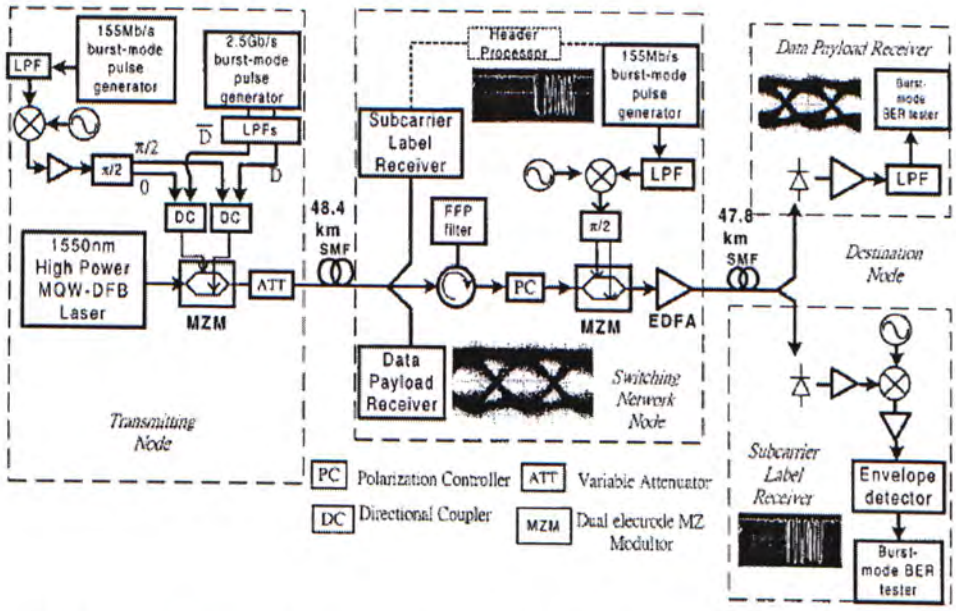

Figure 2.15 Experimental Setup for NCTU-Telecordia testbed. (Adapted from Ref [11])

2.2.4 Code-division OMPLS scheme

Recent progress in high bit rate optical code division multiplexing (OCDM) opens a new way to use optical codes as the optical labels [13]. This is a novel approach in that it eliminates any logic operation in the table look-up, which has been the toughest challenge for optical processing, but it only requires optical correlation [13].

In general, code-division optical encoding schemes are classified into coherent and coherent approaches according to the degree of coherence of the light source. Thus, there are also two alternative solutions to incorporate OCDM into code-division OMPLS scheme.

2.2.4.1 Coherent Code-Division Label Scheme

The first one is the coherent approach proposed by Kitayama [14]. The operation principle of this approach is shown in Figure 2.16.

For this proposal, label swapping can be implemented in all-optical domain. The schematic diagram of photonic label swapping is shown in Figure 2.17. Based on XPM effect, the operation principle is illustrated in Figure 2.18. When the input signal pulse propagates along with the control optical pulse in an optical fiber, the refractive index seen by the input optical pulse is changed by the control pulse because of the cross phase modulation (XPM). As a result, the input signal pulse experiences a phase shift Φ_{max}, which is determined by both the intensity of the control light and the interaction length. By appropriately setting the wavelength and intensity of the control pulse, the signal pulse will have a desired phase shift at the output of the fiber. For example, to swap the 4-chip long BPSK optical code, [0000] to a different code [00$\pi\pi$], as shown in Figure 2.18, the intensity of the control pulses have to be set so that the total phase shift becomes π. Therefore, all-optical label swapping is realized by using control pulses to change the phase of the signal pulses.

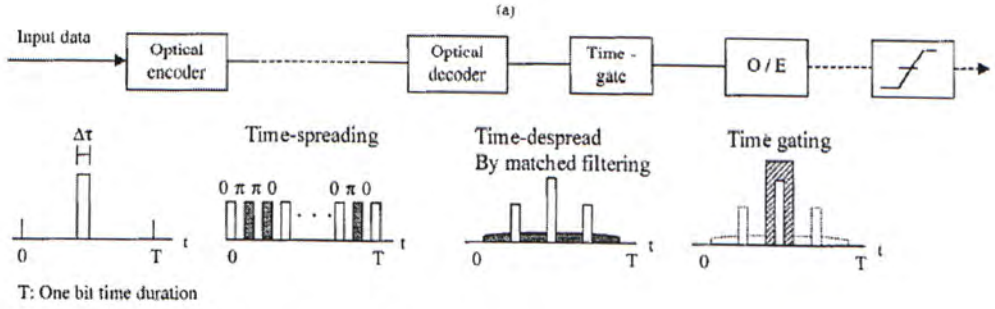

Figure 2. 16 Operation principle of coherent optical code division multiplexing (OCDM). (Adapted from Ref [14])

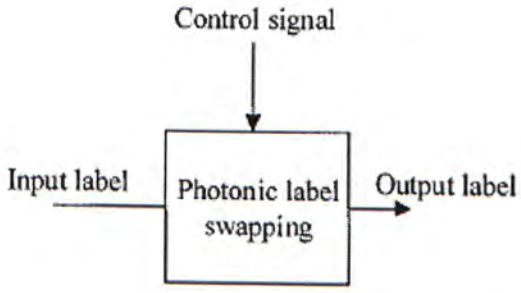

Figure 2.17 Architecture of photonic label swapping for code-division label. (Adapted from Ref [14])

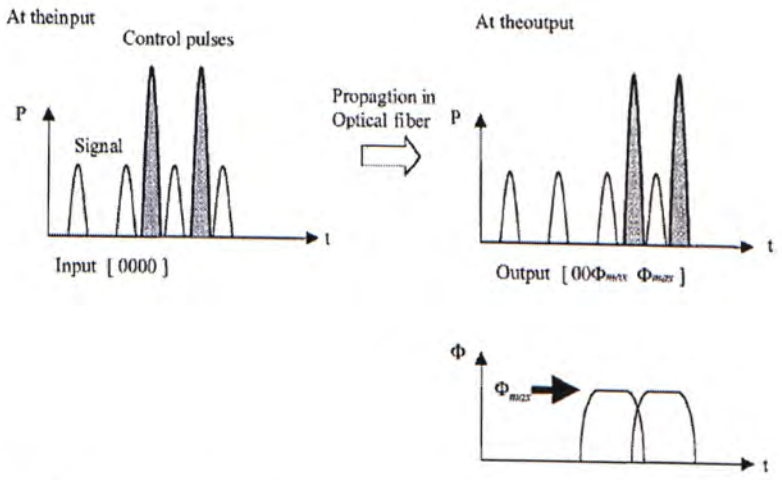

Figure 2.18 Principle of photonic label swapping for code-division label. (Adapted from Ref [14])

2.2.4.2 Noncoherent Code-Division Label Scheme

The noncoherent approach was proposed in reference [15-16].As shown in Figure 2.3(d), data bit is modulated by optical orthogonal code (OOC) in time domain, that is, when data bit is ONE, an OOC is sent out, and when data bit is ZERO, no code is sent or the complementary format of the OOC is sent. This OOC also performs as the optical label, which can be used to forward the IP packet to its destination.

In reference [15], the sequence inversion keyed (SIK) direct spread (DS) code division multiple-access (CDMA) scheme is considered. In an optical SIK system, the data bits are modulated either by a unipolar signature sequence C_i or its complement $\overline{C_i}$, depending on whether the transmitting bit is ZERO or ONE, respectively. With this property, all-optical label swapping can be implemented by code conversion, which can be realized by processing the incoming code label and a control code with an optical XOR gate.

In the routing node, the input signal is a SIK DS-CDMA signal modulated by the code C_i, corresponding to the Virtual Optical Code Channel (VOCC) *VOCC*(*i*). An optical code converter is used to convert the code C_i to code C_j, corresponding to the routing from *VOCC*(*i*) to *VOCC*(*j*). Here the concept of conversion code Q_{ij} is introduced. By processing the input signal with Q_{ij}, the information carried in the *VOCC*(*i*) can be coupled to the *VOCC*(*j*). Thus our proposed code converter realizes the all-optical CDMA switching function.

For the scheme, the conversion code Q_{ij} must have two properties of $C_i \oplus Q_{ij} = C_j$ and $\overline{C_i} \oplus Q_{ij} = \overline{C_j}$. It is found that with $Q_{ij} = C_i \oplus C_j$,

$$C_i \oplus Q_{ij} = C_i \oplus (C_i \oplus C_j) = C_i \oplus C_i \oplus C_j = 0 \oplus C_j = C_j$$

$$\overline{C_i} \oplus Q_{ij} = \overline{C_i} \oplus (C_i \oplus C_j) = \overline{C_i} \oplus C_i \oplus C_j = 1 \oplus C_j = \overline{C_j}$$

Thus the unique conversion code $Q_{ij} = C_i \oplus C_j$ can facilitate the routing function from *VOCC(i)* to *VOCC(j)*. For example, for the 4-chip Walsh codes having C_1=[1 0 1 0] and C_2=[1 1 0 0], the code conversion function from C_1 to C_2 is verified by

$$Q_{12} = C_1 \oplus C_2 = [0 \quad 1 \quad 1 \quad 0]$$

$$C_1 \oplus Q_{12} = [1 \quad 0 \quad 1 \quad 0] \oplus [0 \quad 1 \quad 1 \quad 0] = [1 \quad 1 \quad 0 \quad 0] = C_2$$
$$\overline{C_1} \oplus Q_{12} = [0 \quad 1 \quad 0 \quad 1] \oplus [0 \quad 1 \quad 1 \quad 0] = [0 \quad 0 \quad 1 \quad 1] = \overline{C_2}$$

Based on this principle, a proposed code converter is shown in Figure 2.19.

The code converter is a modified TOAD that has two arms of control pulse input. One is the routing node's input channel code C_i, and the other is the conversion code Q_{ij}. These two signals are of the same wavelength, whereas the XOR clock is on a different wavelength, such that they can be separated by an optical filter at the output port. After the clock enters the loop through the main coupler, it splits into two pulses, a clockwise (CW) and a counter-clockwise (CCW) pulse. Each of these two pulses passes through the SOA once, and returns to the main coupler at the same time. When the two control arms have the same signal level, 1 or 0, the CW and CCW pulses will experience the same transmission properties of the SOA. The clock train is then totally reflected into the input port and no pulse appears in the output port. On the other hand, if one of the two control arms has a 1 level and the other has a 0 level, the CW and CCW pulses will experience different transmission properties of the SOA. The clock pulse train will come out from the output port of the TOAD when the phase difference between the CW and CCW pulses is π. Thus, the output channel code $C_j = C_i \oplus Q_{ij}$ is obtained at the output port of the code converter.

Another alternative code converter based on the same principle is shown in Figure 2.20.

However, none of these reported code-converted approaches investigates the fundamental issue of multi-access interference (MAI), the cross-correlation between the selected code channel and the other co-propagation code channels. Thus, in

reference [16], we propose a switch fabric for OOC MPLS core router, which take the MAI into consideration. In this thesis, I would like to investigate and discuss in detail on the architecture and scalability of the OOC MPLS core router.

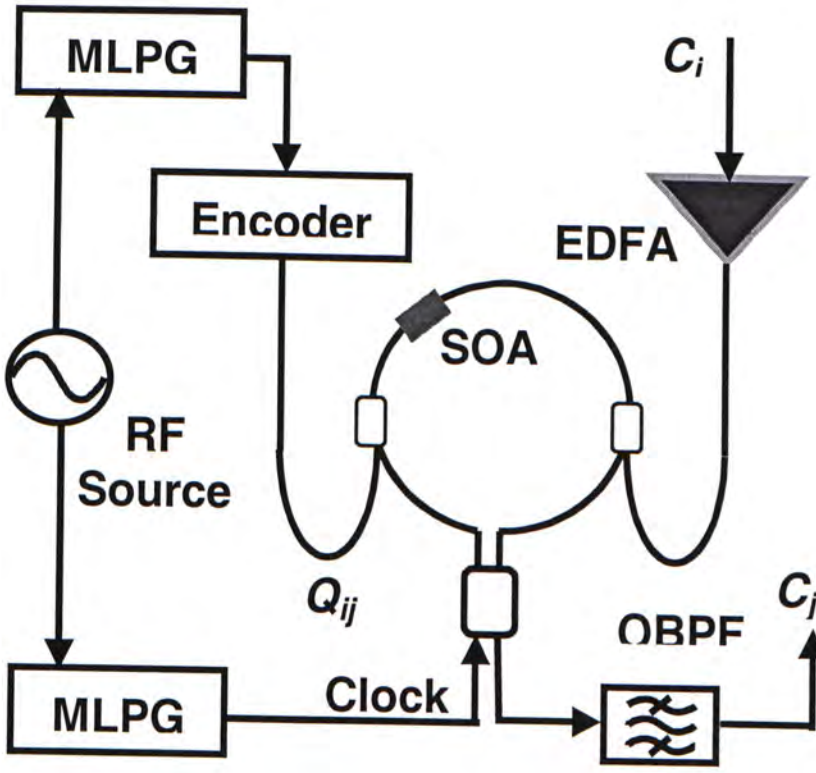

Figure 2. 19 A proposed code converter for OCDM OMPLS network.

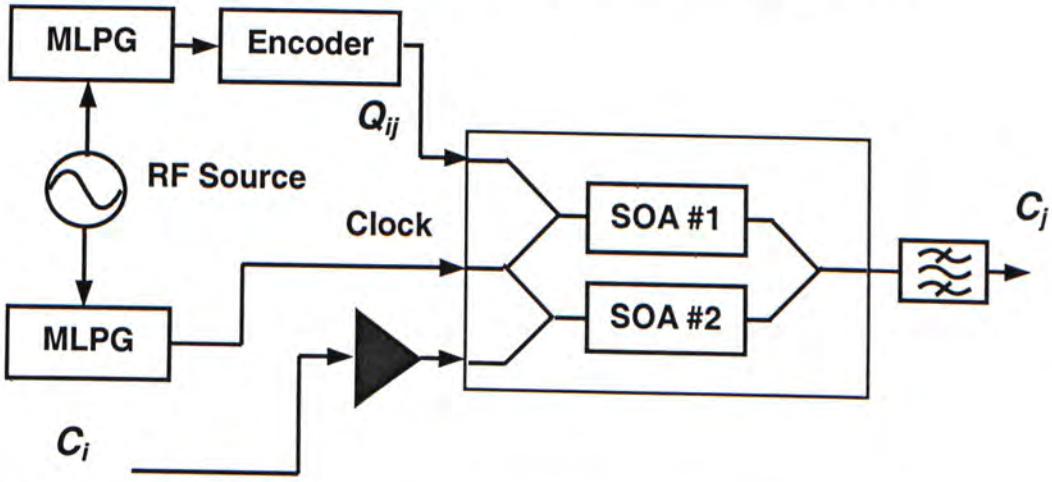

Figure 2. 20 Another proposed code converter for OCDM OMPLS network.

2.3 Reference

[1] Daniel J. Blumenthal, et al, " All-Optical Label Swapping Networks and Technologies", IEEE/LEOS Journal of Lightwave Technology, Vol. 18, No. 12, pp. 2058-2075, December 2000.

[2] C. A. Bracket, " Dense wavelength division multiplexing networks: Principles and Applications", IEEE Journal of Selected Areas of Communication, Vol. 8, No. 8, pp. 948-964, August 1990.

[3] P. Toliver, K.-L, Deng, I. Glesk, and P. R. Prucnal, " Simultaneous optical compression and decompression of 100-Gb/s OTDM packets using a signel bi-directional optical delay line lattice", IEEE Photonic Technology Letters, Co. 11, pp. 1183-1185, September 1999.

[4] K. Kitayama, " Code Division Multiplexing Lightwave Networks Based upon Optical Code Converter", IEEE Journal of Selected Areas in Communications, Vol. 16, No. 7, pp. 1309-1319, September 1998.

[5] A. Viswanathan, N. Felfman, Z. Wang and R. Callon, " Evolution of multiprotocol label switching", IEEE Communication Magazine, Vol. 36, pp. 165-173, May 1998.

[6] D. J. Blumenthal, P. R. Prucnal and J. R. Sauer, " Photonic Packet Switches: Architectures and Experimental Implementations", Proceedings of the IEEE, Vol. 82, No. 11, pp. 1650-1667, November 1994.

[7] T. Fjelde, A. Kloch and D. Wolfson, " Novel Scheme for Efficient Label-Swapping Using Simple XOR Gate", Proceeding of ECOC'2000, Vol. 4, pp. 63-64, September 2000.

[8] N. Wada, H. Harai, W. Chujo and F. Kubota, " Photonic Packet Switching based on Multi-wavelength Label Switching Using Fiber Bragg Gratings", ECOC'2000, paper P10.4.6, Sep. 3-7, 2000, Munich, Germany.

[9] A. Carena, M.D. Vaughn, R. Gagudino, M. Shell and D. J. Blumenthal, " OPERA: An Optical Packet Experimental Routing Architecture with Label Swapping

Capability", IEEE/LEOS Journal of Lightwave Technology. Vol. 16, No. 12, pp. 2135-2145, December 1998.

[10] S. J. B. Yoo, Hyuek J. L, Srikanth Vaidianathan, Katsunari Okamoto and Shin, Kamei, " Optical-Label Switching and Routing by Rapidly Tunable Wavelength Conversion and Uniform Loss Cyclic Frequency Array-Waveguide Grating", Proceeding of OFC'2001, Paper WDD49, March 17-22, California, USA.

[11] Y. M. Lin, W. I. Way and G. K Chang, " A Novel Optical Label Swapping Technique Using Erasable Optical Single-Sideband Subcarrier Label", IEEE Photonics Technology Letters, Vol. 12, No. 8, August 2000.

[12] G. H. Smith and D. Novak, " Broad-band millimeter-wave (18 GHz) fiber-wireless transmission system suing electrical and optical SSB modulation to overcome dispersion effects", IEEE Photonics Technology Letters, pp. 141-143, January 1998.

[13] N. Wada and K. Kitayama, " 10 Gb/s optical code division multiplexing using 8-chip optical bipolar code and coherent detection", IEEE/LOES Journal of Lightwave Technology, Vol. 17, pp. 1758-1765, 1999.

[14] K. Kitayama, et al, " Architectural Considerations for Photonic IP Router Based upon Optical Code Correlation", IEEE/LEOS Journal of Lightwave Technology, Vol. 18, No. 12, pp. 1834-1844, December 2000.

[15] Y.G. Wen, L. K. Chen, K. P. Ho and F. Tong, " An All-Optical Code Converter Scheme for OCDM Routing Networks", ECOC'2000, paper P4.5, September 3-7, 2000, Munich Germany.

[16] Y. G. Wen, L. K Chen and F. Tong, " Fundamental Limitation and Optimization on Optical Code Conversion for WDM Packet Switching Networks", Proceeding of OFC'2001, paper TUv-5, March 17-22, California, USA.

Chapter 3

Architecture of OOC-based OMPLS network

3.1 Infrastructure of OOC-label switch router (code converter)

As mentioned in chapter 2, several optical MPLS schemes were proposed previously, such as, time-division label [1], wavelength-division label [2], frequency-division label [3] and code-division label [4]. In particular, the code-division label scheme has the advantages of employing optical orthogonal code (OOC) as label and label swapping by code conversion. Thus, it alleviates the interference from other labels and noises due to the orthogonality of optical code.

There are two approaches to use code-division label, that is, coherent scheme (Bipolar code and phase modulation) and noncoherent scheme (OOC code and intensity modulation). So far, for these approaches, all reported code conversion schemes could be classified intro three different approaches. The first [5] is based on coherent method, albeit its application is limited by fiber dispersion and polarization disturbance. The second [6] on relies on look-up table and requires extensive, undesirable OE-EO processing. The third [7] scheme uses an all-optical logic XOR gate to implement code converter. Nevertheless, none of these reported code-converter deals with the fundamental issue of multi-access interference (MAI), the cross-correlation between the selected code channel and other co-propagation channels.

Due to the intrinsic unipolar property of OOC set, MAI cannot be eliminated and will degrade the performance of packet switching networks. Thus, in this thesis, a MAI-suppression multi-channel code converter will be proposed, and the detrimental effects of MAI will be investigated.

3.1.1 Architecture of the Proposed Code Converter

Fig. 3.1 shows a generic optical switch fabric for the MAI-suppression multi-channel code conversion. The received optical signals in a single input fiber are composite signals consisting of WDM wavelength-code channels (λ, C), with each channel uniquely described by a particular wavelength $\lambda_i \quad i = 1,2,\cdots N$ and a particular OOC $c_i \quad i = 1,2,\cdots M$ at any given time. The composite signals are first separated in the wavelength domain by an optical wavelength demultiplexer, for instance, an array waveguide grating (AWG). Following the AWG, the M code channels in each of the demultiplexed wavelength are decorrelated by M decoders, each of which functions as a dedicate correlator. Output from each decoder will feed into a time-gate-intensity-threshold (TGIT) device. The TGIT device is necessary in order to differentiate the auto-correlation peaks from its sub-peaks and cross-correlation peaks, all generated from the decorrelated optical pulse train. Accordingly, for a received data of ONE/ZERO bit, the corresponding auto-correlation peak is an optical pulse/null. It should also be noted that the TGIT device could be configured to perform wavelength conversion, thus offering additional function of data routing (more details in section 3.2).

Following the threshold device array is an optical space switch, which can be a non-blocking three-stage Clos network switch (Fig. 3.2) responsible for routing the optical pulses to different output ports. For channel add-drop, the channel is routed to a drop port. A new data channel is inserted through the add port of the optical space switch. For optical signal forwarding function, the optical pulse decoded from code channel i is routed to the input of the encoder of code channel j designated for code j. Finally, the outputs of the encoder array are multiplexed by an AWG multiplexer into the output fiber, and forwarded to next switching node.

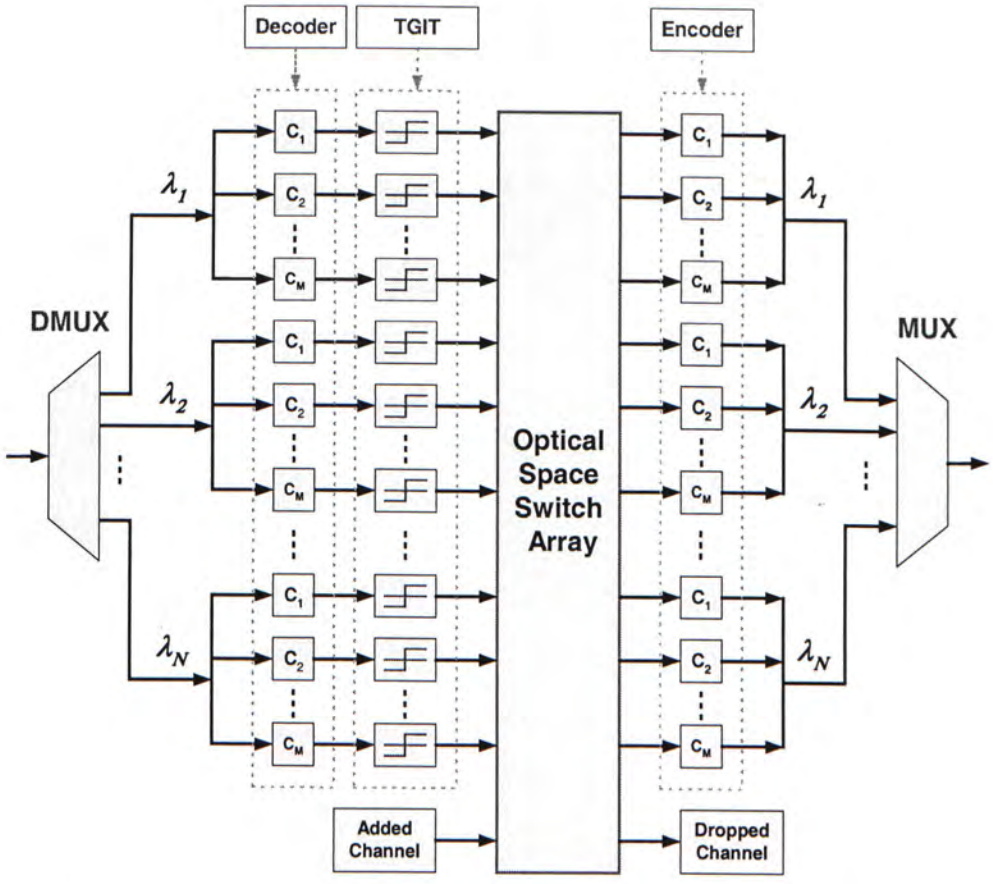

Figure 3.1 The schematic diagram of the proposed photonic code-based MPLS core router fabric. TGIT: Time-Gating-Intensity-Thresholding Device

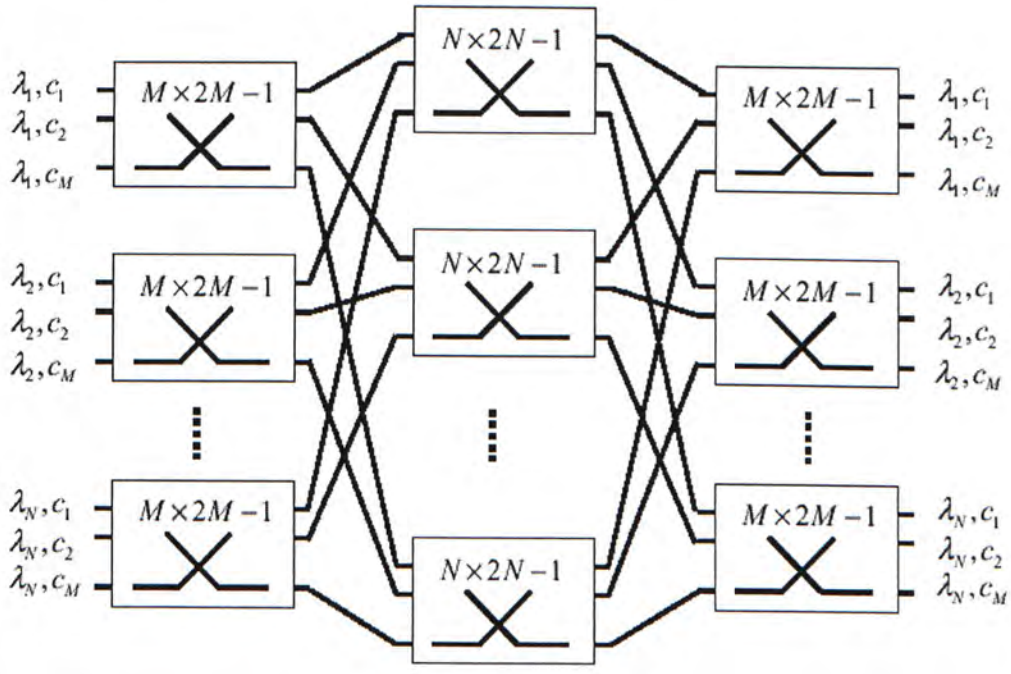

Figure 3.2 The streamlined diagram of a three-stage Clos network for optical space switch.

3.1.2 Enhancement of the Code Converter

The above code converter architecture is inherently suitable for one in/output fiber circuit-switch based optical label network. In order to support more practical system, the proposed architecture can be enhanced to various robust versions.

Multi-fiber Extension

For a practical optical label router, it is common that it has two or more in/output fibers. Therefore, our proposal can be extended to work in this scenario. Conceptually, it can be implemented by adding another dimension over wavelength/code, resulting in the fiber/wavelength/code dimensions. For the multi-fiber nodes, every individual input fiber is first connected to an AWG device to separate different wavelength channels. Then, the channels of the same wavelength from different input fibers go through the code processor array designed for a certain wavelength as usual. In the code processor array, the fiber dimension is transparent. Before the output is combined in the final AWG device, the control component will decide the output fiber for every wavelength-code signal.

Output Contention Resolution

In a packet-switched network, each packet has to go through a number of switches to reach its destination. When the packets are being switched, contention occurs whenever two or more packets are trying to leave the switch from the same output port. There are three types of typical contention resolutions: optical buffering, deflection routing, and wavelength/code conversion. For our proposal, it can perform wavelength/code conversion inherently, thus offering an inherent reduction of contention. In order to employ our proposed architecture for packet-based WDM network efficiently, we can incorporate another type of contention resolution, such as optical buffering or deflection routing. Combined with the consistent wavelength/code conversion, it will offer the network designers more choice and flexibility. As an example, in a switch node with both wavelength conversion and

buffering, the input stage demultiplexes wavelength channels and the control components locate available wavelengths on certain output ports. The nonblocking space switch selects the output port or appropriate delay lines, which are used to implement optical buffer. With the combined contention resolutions, it can reduce the number of optical buffers or reduce packet loss probability [20].

3.2 Implementation of the OOC code converter

3.2.1 Encoders/Decoders

For the systems with optical code-division label, the coding architecture of optical encoders/decoders is a very important factor to be considered. For example, power loss in encoders/decoders will impose restrictions on the power budget, the length of sequences and the number of subscribers; the length of delays imposes restrictions on the size and cost of such a system. Therefore, much attention [8-10] has been paid to the design of good coding architectures to facilitate the implementation of OCDM system.

In general, OOC encoders/decoders proposed previously can be classified into three categories: (1) all-parallel approach [11], (2) all-serial approach [12] and (3) serial-to-parallel approach.

3.2.1.1 All-parallel encoders/decoders

When OCDM was first proposed, all-parallel encoder/decoder (Figure 3.3) was the hottest topic in this research field. Its operational principle is very simple: at the first stage, pulse source is split into N copies by the optical splitter; at the second stage, every individual copy of pulse source passes through an optical delay line of various lengths with a step size τ from the 1^{st} path to the N^{th} path; then at the third stage, electrical address signal is used to control the optical switch array that passes the optical signal corresponding to code bit ONE and cuts off the optical signal corresponding to code bit ZERO; finally, at the fourth stage, the optical combiner combines all the optical signals to finish the coding processing. For the decoder, the same structure can be used in the same way.

The advantages of the architecture are obvious. It is a basic architecture for OOC encoders/decoders, with less implementation complexity. Though it originally proposed for prime codes, it is suitable for any OOC family. However, it needs large

number of delay lines and switches. Moreover, it can only be used to encode fixed length OOC.

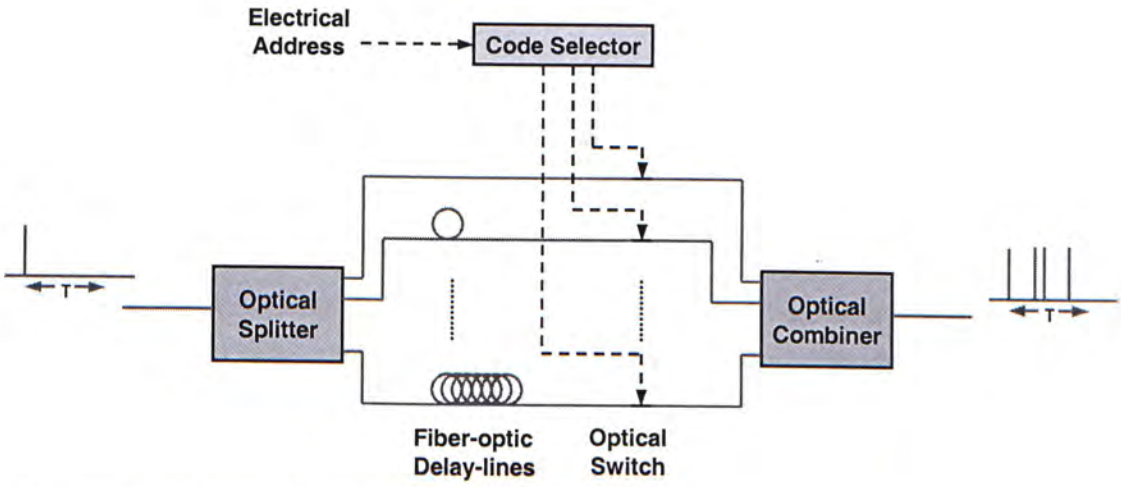

Figure 3.3 All-parallel encoder.

3.2.1.2 All-serial encoders/decoders

Recent research on the use of fiber-optic lattice signal processing provided a better coding architecture for optical CDMA. Figure 3.4 shows the block diagram of the modified 2^n encoder, where an all-serial architecture is used for code sequence generation, selection and correlation.

In each encoder, code sequence generation and selection are provided by a serial combination of 2x2 switches and unit delays. The unit delays provide delays equal to the duration of a single chip and are made of either optical fibers or waveguides. In general, the encoder is basically constructed with a number of switching stages, each with a 2x2 switch and unit delay. Each 2x2 switch can be configured into two possible states (i.e., cross-bar or straight-through) according to its DC bias voltage, fed by the electronic address selector. The cross-bar state allows optical pulses to mix and to split inside a 2x2 switch, while the straight-through state allows optical pulses to pass through the switch without changes. At the input of the encoder, a narrow laser pulse is first split into two pulsed by a passive coupler. One of the pulses is delayed and the amount of delays is accumulated as the pulse passing through straight-through-state 2x2 switches. After the proper amount of delays is obtained, the delayed pulse combines with non-delayed one at a cross-bar-state 2x2 switch. At the same time, the two pulses then split into four pulses (i.e., two pulses in each path) and the process repeats until the desired number of ones are generated.

Because of the serial structure, 2^n code is generated with n 2x2 switches in the cross-bar states and the rest in the straight-through states. Apparently, the total number of switches should depend on the sequence length N that is usually a large number. Actually, by carefully choosing the amount of delay (i.e., using non-unit delay) in each stage, the required number of switches can be reduced substantially.

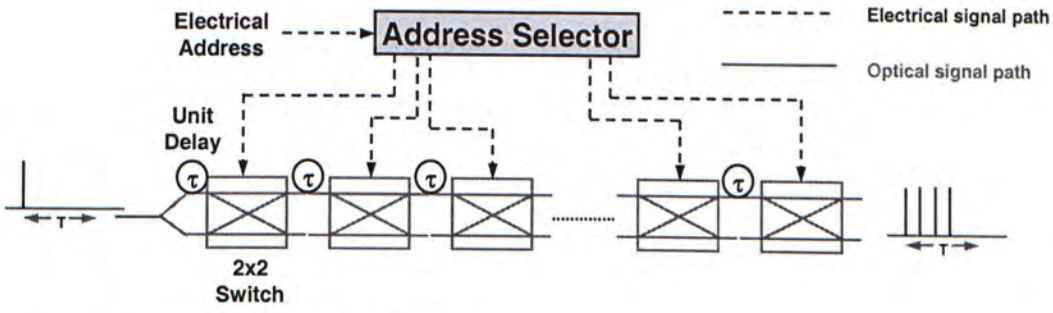

Figure 3.4 All-serial encoder/decoder.

3.2.1.3 Serial-to-parallel encoders/decoders

For all-parallel approach, a large number of delay lines and switches are needed, and for all-serial encoder, the number of switches is also very large. This cost will limit their application in practical systems. In order to implement the label encoder/decoder economically, we propose another approach called serial-to-parallel encoder/decoder.

The schematic diagram of serial-to-parallel encoder is shown in Figure 3.5. The encoder includes three unit delay lines, four switches, serial-to-parallel interleaver and an optical combiner. At the input of the encoder, an optical pulse source is fed. The interleaver partitions the incoming code sequence into four sub-code sequences via serial-to-parallel processing, for example, the incoming code sequence $C_1C_2C_3C_4C_5C_6C_7C_1C_2C_3C_4C_5C_6\cdots$, after the interleaver, we have four sub-code sequences: $C_1C_5C_2\cdots$, $C_2C_6C_3\cdots$, $C_3C_7C_4\cdots$, $C_4C_1C_5\cdots$. These four sub-code sequences are used to control the switches. When the pulse passes through the delay line path, four copies of the pulse are tapped out to pass through the switches. When the driving bit is ONE, the switch let the pulse through; otherwise, the pulse is blocked. The optical combiner combines the outputs of the four switching paths to finish the coding processing.

Compared with the all-parallel and all-serial encoders, the serial-to-parallel encoder is more economically practicable. The following advantages are obvious: (1) it needs only three unit delay lines, and is independent of the code length; (2) it needs only four switches, which is independent of the code length N; (3) it is suitable for OOC family of any format and any length; (4) it relaxes the requirement for the switching rate by four times and (5) it can be integrated with the optoelectronics technology. Of course, the encoder requires more synchronization among the four sub-sequences.

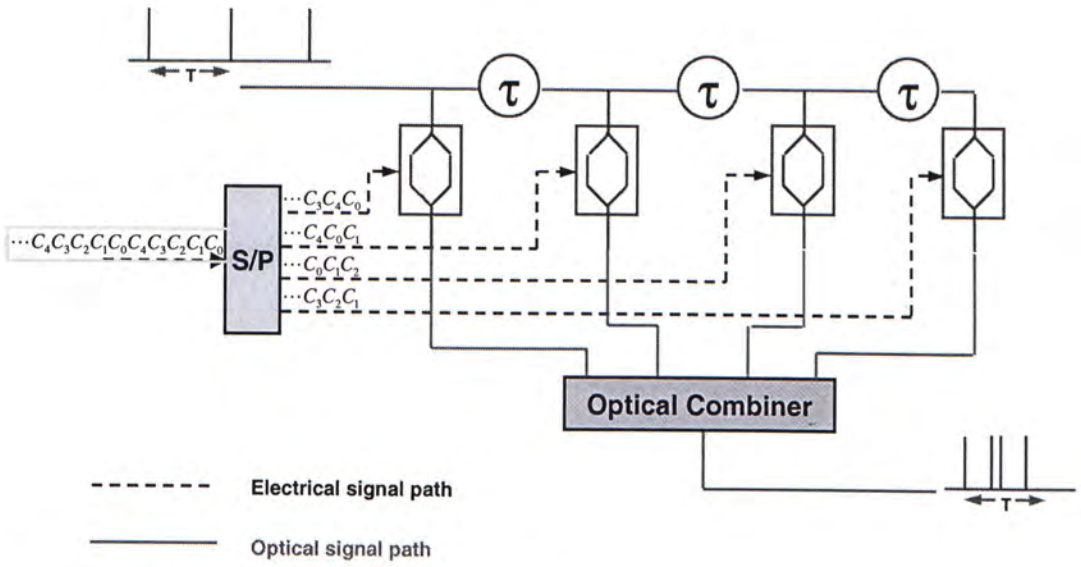

Figure 3.5 Serial-to-Parallel encoder/decoder.

3.2.1.4 Comparison the three kinds of encoders/decoders

In order to investigate the performance of these three kinds of encoders/decoders, we compare five parameters of them under the same condition. The five parameters are: (1) the number of switches, (2) the number of unit delay line, (3) switching time, (4) power loss and (5) encoded extinction ratio.

In Figure 3.6, the three kinds of encoders are compared respect to five parameters, where N is the code length, n is the parameter of 2^n code, T_0 is the chip width, P is the code weight, r_0 is the original extinction ratio and a is the degraded factor by a switch. From the comparison, it can be known that the serial-to-parallel encoder approach outperforms both the all-parallel encoder and the all-serial encoder in implementation practicability.

For our proposed OOC MPLS network, the serial-to-parallel encoder/decoder should be the first candidate for label processing.

	All-parallel Encoder	All-serial Encoder	Serial-to-Parallel Encoder
Switch Number	N	$O(N)$	4
No.of Unit Delay line	$N^2/2$	$O(N)$	3
Switch rate	T_0	T_0	$4T_0$
Power Loss	$10\log_{10}N$	$30(n+2)$	$30(\log_2 P+2)$
Extinction Ratio	r_0*a	r_0*a^n	r_0*a

Figure 3.6 Comparison of three encoder/decoder approaches. O(N): the number increases with the larger N.

3.2.2 Time-Gate-Intensity-Threshold (TGIT) Device

As with all optical networks, chromatic dispersion [13] is one of the key issues that corrupts the transmitted signal and limits the cascadability of the networks. It is even worse in OCDMA systems, where the chip rate is generally L times of the effective data rate due to the processing gain. Another critical issue for OCDM label network is the Mutli-Access Interference (MAI) and sidelobes of the auto-correlation of the code, which can also degrade the system performance. Therefore, in our design, we must have some mechanisms to combat dispersion and suppress sidelobes.

In order to combat chromatic dispersion and suppress sidelobes, a device called Time-Gating-Intensity-Thresholding (TGIT) device is proposed. It is a two-stage device, the first stage is dedicated for time gating, and the second stage is dedicated for intensity thresholding. In Figure 3.7, a schematic diagram of TGIT is shown with its operational principle.

As shown in Figure 3.7, the time-gating section is actually a pulse-sampling device that selects the autocorrelation central spike. Thus, it can be used to improve the pattern recognition contrast for the distorted waveform, making the transmission more immune to the effects of dispersion. Time-gating is an all-optical process, which essentially operates as a time-domain demultiplexer. Therefore, time-gating section also suppresses any sidelobes originated from the autocorrelation of the optical code, and reduces the effect of any interfering channels outside the time frame of the main autocorrelation peak.

For our design, we need an optical pulse as the pulse source of the final encoding stage when data bit is ONE, and this optical pulse should not come out for data bit ZERO. Thus, in the TGIT device, the second section performs optical intensity threshold processing. As shown in Figure 3.7 (b) and (c), when received data bit is ONE, the demultiplexed central peak is over the threshold value, then after the threshold device, an optical pulse can be generated for the final encoding stage. On the other case, when received data bit is ZERO, the demultiplexed central peak is

below the threshold value, and then no optical pulse will come up after the threshold device. For optical threshold device, we can also use optical time-domain multiplexer to implement. The intensity-thresholding section also suppresses the residue sidelobes due to the non-ideal performance of time-gate stage.

With a two-stage TGIT device, we can combat the detrimental effects of chromatic dispersion and suppress the sidelobes of the autocorrelation and the cross-correlations [14]. Moreover, with a two-stage architecture, code conversion and wavelength conversion becomes independent. This provides more flexibility to our proposal. This issue is reiterated later in the implementation of TGIT device.

As we mentioned above, both the time-gating section and the intensity-thresholding section of TGIT device can be implemented with an optical time-domain multiplexer. Currently, there are mainly four candidates for optical time-domain multiplexer: (1) Nonlinear Optical Loop Mirror (NOLM)[15], (2) Terahertz Optical Asymmetric Demultiplexer (TOAD)[16], (3) Ultrafast Nonlinear Interferometer (UNI)[17] and (4) Mach-Zehnder Interferometer (MZI) [18]. For implementing the TGIT device, we can choose them according to the data/chip rate, cost and flexibility. In the following, as an example, the architecture, the operational principle and the features of a two-MZI-based TGIT device are investigated.

Figure 3.8 shows a TGIT device architect with two MZIs. The first MZI works as the time-gating device, the second MZI works as the intensity-thresholding device. The output of the decoder is fed into the time-gating device. The MZI is driven with a Mode-Locked Laser (MLL) operating at an intermediate wavelength λ_{int}. After the band-pass filter (BPF), the central peak of the decoder output is demultiplexed and converted to wavelength λ_{int}, and the sidelobes are much suppressed at the same time. On the second stage-threshold device, the demultiplexed central peak is used as the control pulses of the MZI device, and another MLL (wavelength λ_{new}) is used as the new pulse source. Then after the second BPF, the demultiplexed pulse is enhanced or suppressed according to the comparison between the intensity and the threshold

value. Meanwhile, the final output is converted to a new wavelength. If we do not need wavelength conversion in the design, we can set the new wavelength λ_{new} equal to the original wavelength, otherwise, we can choose the new wavelength as the desired wavelength determined by the control plane. Therefore, code conversion and wavelength conversion can be realized independently.

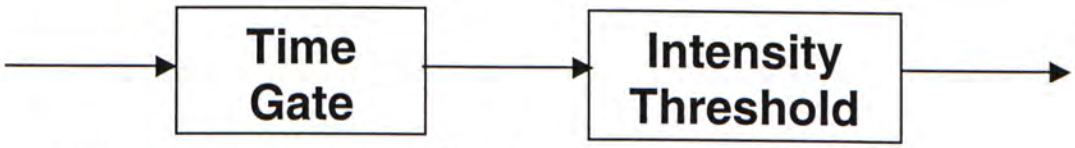

(a) A schematic diagram of TGIT device

(b) The sequence flow of the matched code receiver

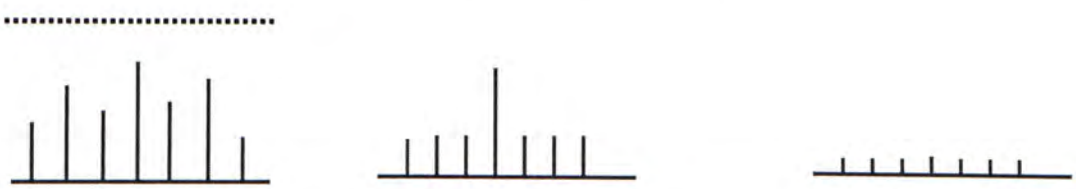

(c) The sequence flow of the unmatched code receiver

Figure 3.7 Schematic diagram of TGIT device with its operational principle.

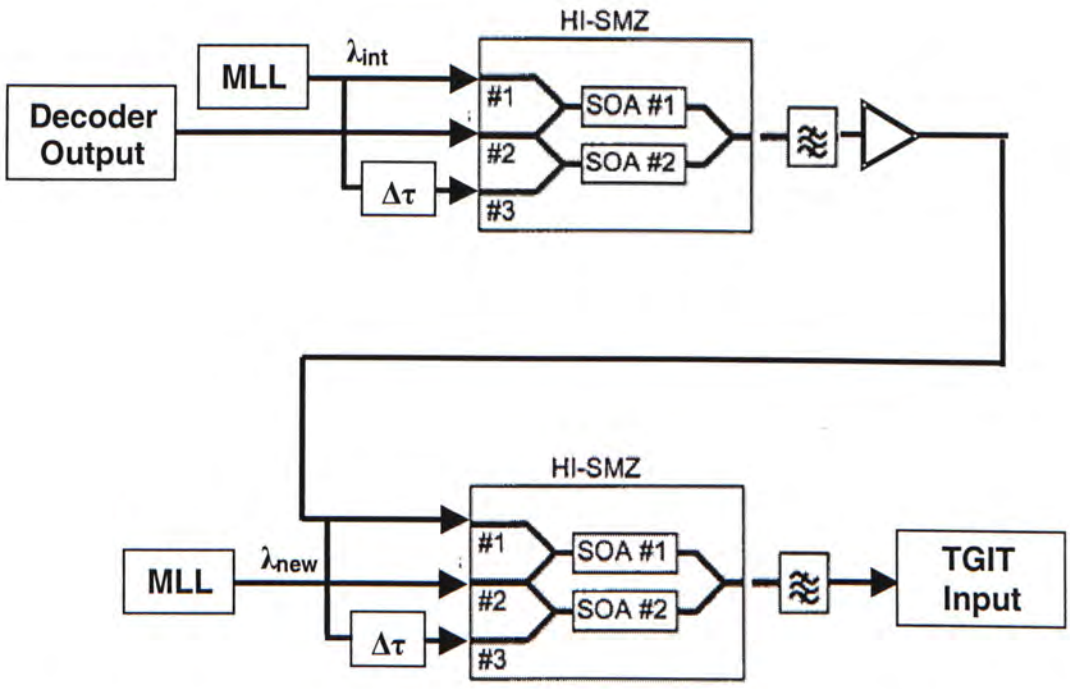

Figure 3.8 The architecture of a two-stage Time-Gating-Intensity-Thresholding (TGIT) device based on two Mach-Zehnder Interferometers. SOA: semiconductor optical amplifier, MLL: mode-locked laser, HI-SMZ: hybrid-integrated symmetric Mach-Zehnder, λ_{int}: intermediate wavelength, λ_{new}: new wavelength.

3.2.3 Optical Space Switch Array

3.2.3.1 All-optical Space Switch

Currently, optical switch fabric can be classified into two approaches: opaque approach with OEO processing and transparent approach without OEO processing. In the following, the two approaches are described and their pros and cons are discussed.

In opaque approach, optical signals are converted back into electrical domain so that their route across the middle of the switch can be handled by conventional application specific integrated circuits (ASIC) or FPGA. Right now, the optical switches being provided by Ciena Corp., Sycamore Networks Inc., and Tellium Inc. can be classified into this category.

This approach has a lot of advantages. Most notable is to enable the switches to handle smaller bandwidths than whole wavelengths, which supports current market requirements. More over, the electrical cores also make network management easier, because standards are in place and products are available.

However, the explosion in the number of wavelengths in telecom networks, resulting from the deployment of DWDM (dense wavelength-division multiplexing), cannot be handled by conventional electrical cores. Even until recently, it is reported that state-of-the-art ASIC technology would not support anything more than a 512-by-512-port electrical core, and carriers have been saying they need at least double this capacity [19].

On the other hand, all-optical switches, which do not convert light pulses back into electrical domain to process, do not suffer this limitation. Therefore, transparent approaches are gaining much attention these days. Nowadays, plans for all-optical switches with more than 1,000 ports have been announced by a number of vendors, such as, Calient Networks, OMM Inc., Onix Microsytems Inc., and Nortel Networks Corp.

Another advantage of all-optical switches is that it can eliminate the need for optical-electrical-optical (OEO) processing in the network, saving carriers millions in both the network core and metro edge. In addition, all-optical switches make networks more future-proof. Carriers will not have to upgrade equipment to support higher transmission speeds, so they will be able to catch up with advances in technology more easily and quickly. Finally, it enables faster bandwidth provisioning, with new service can be provided in days, rather than months.

However, it is a little different in practice. Currently, vendors are trying to design larger scale electrical cores. For example, Brightlink Networks Inc. announced its switch would eventually scale to many thousands of ports; and Velio Communications Inc. announced some electrical switching fabric developments that could support cores of a similar scale. This may delay the domination of deployment of all-optical switches.

All the same, the idea of all-optical networks will succeed in combating with opaque approach. The folk developing fabric for all-optical switches have come a long way, but they've still got a long haul ahead of them to convince carriers to use their technologies. For our proposal, transparent approach is preferable.

3.2.3.2 Optical switching technologies

Currently, there is a wide range of different technologies proposed for the switch fabric of all-optical switches. However, it is unlikely that one particular technology will dominate, because optical switches are likely to be used for a wide range of applications. What is exactly the right switching fabric in one place could be exactly the wrong switching fabric for somewhere else.

Here we list a few of the ways in which optical switch fabrics can be measured: Matrix Size, Scalability, Granularity, Switching Speed and Loss. For our proposed, we should evaluate all the available technologies in these ways according to the application environments. Therefore, in the following, the overview and comparison of the current optical switch fabric technology is quote from [19], including (1) Micro-electro-mechanical systems (MEMS), (2) Liquid Crystals, (3) Bubbles, (4) Thermo-Optics, (5) Holograms, (6) Liquid Gratings and (7) Acousto-Optics.

3.2.3.2.1 Scalability

Technology	Key characteristics: Scalability
MEMS	1. For 2D subsystem, 32x32 ports are maximum number. Multiple subsystems can be linked together up to 512x512 ports. 2. For 3D subsystem, the solution that can support thousands of ports has been developed, but this hasn't been proven experimentally.
Liquid Crystal	1. In theory, Good. 2. In practice, only modestly sized (80 wavelength maximum) devices can be developed by vendors.
Bubbles	1. The prototype of 32x32-port and 32x16-port subsystems has been developed by Agilent. 2. Larger switch cores can be created by connecting multiple these subsystems.
Thermo-Optics	1. The largest switch is a 16x16 port-device by NTT Electronics. 2. Size is limited not by optical losses, but by the power consumed in switching.

Holograms	By Trellis Photonics, up to 1920 wavelength per switch can be supported.
Liquid Gratings	1. Small switches (1x1, 2x2) are under research in DigiLens. 2. To scale the technology will probably require cascading smaller devices.
Acousto-Optics	1. Current crystal-based developments target a maximum of 256x256 ports. 2. Fused coupler developments probably target smaller switches.

3.2.3.2.2. Switching speed

Technology	**Key characteristics: Switching speed**
MEMS	By OMM Inc., 10 milliseconds are typical for its 4x4 and 8x8 switches. Switching time increases to 20ms for the larger 16x16 device.
Liquid Crystal	Problematic. Switching speeds can be improved by heating the crystals to make them less viscous.
Bubbles	10 milliseconds, by Agilent.
Thermo-Optics	1. Depends on how fast it is possible to heat the material. 2. For Polymer switches, a switching speed of a few milliseconds can be achieved. 3. For Silica, the number is around 6 to 8ms, though startup Lynx Photonic Networks claims switching speeds of 2ms and expects to reduce this to 1ms.
Holograms	Very fast. It is reported by Trellis Photonics that it can switch from one wavelength to another in a few nanoseconds.
Liquid Gratings	100 microseconds were reported by DigiLens. Only holograms are faster than liquid gratings.
Acousto-Optics	Varies from 500 nanoseconds to 10 microseconds

3.2.3.2.3 Reliability

Technology	Key characteristics: Reliability
MEMS	Due to moving parts, reliability is limited by mechanisms sticking, wearing out, or getting damaged by vibrations.
Liquid Crystal	Potentially good; no moving parts
Bubbles	Potentially good; no moving parts and the problems of manufacturing large volumes of ink jet pens have already been ironed out. However, unlike an inkjet, the bubbles have to be maintained for extensive periods of time. Agilent says that the bubbles are held in a closed system, so cannot escape (an ink jet uses the bubble to push out the ink). Moreover, the unit is operated at the vapor pressure point -- the temperature and pressure at which both liquid and gas can coexist. As a result, it takes very little heat to create a bubble. Ink jet cartridges don't have to last 20 years.
Thermo-Optics	Potentially good as there are no moving parts. The life of switches is limited by repeated heating and cooling.
Holograms	Potentially good; no moving parts.
Liquid Gratings	Potentially good; no moving parts.
Acousto-Optics	Potentially good; no moving parts.

3.2.3.2.4. Losses

Technology	Key characteristics: Losses
MEMS	By OMM Inc., for 4x4 unit, loses up to 3dB; for the 16x16 unit, up to 7dB. Losses increase substantially if multiple subsystems have to be linked together.
Liquid Crystal	Can be problematic
Bubbles	4.5dB per 32x32 subsystem, by Agilent.
Thermo-Optics	Silica has very low losses. Polymer losses are higher, but there has been a lot of progress in reducing the material loss recently. AlliedSignal claims to have developed a polymer with a loss of less than 1dB per centimeter.

Holograms	Less than 4dB loss for a 240x240 switch by Trellis Photonics.
Liquid Gratings	Very low. DigiLens claims that devices based on Liquid Gratings have optical losses of less than 1dB in total.
Acousto-Optics	Low. Losses of less than 2.5dB for its 1x2 switch by Brimcom.

3.2.3.2.5 Port-to-port repeatability

Technology	**Key characteristics: Port-to-port repeatability**
MEMS	Problematic in large switches, because light may have to travel varying distances between ports. By OMM, this could be as big as 3dB in the 16x16 device, though it is less than 0.5dB for the smaller switches.
Liquid Crystal	The same optical performance is required whether the signal goes from port 1 to port 16, or port 2 to port 15. Potentially problematic in most developments, because light has to be split into two differently polarized beams before passing through the liquid crystals, and then has to be recombined. If the path lengths are slightly different, losses result.
Bubbles	Unknown.
Thermo-Optics	Good
Holograms	Good. In fact Trellis claims there is no path dependency within its switch at all.
Liquid Gratings	Unknown
Acousto-Optics	Unknown

3.2.3.2.6 Cost

Technology	**Key characteristics: Cost**
MEMS	Unknown
Liquid Crystal	Unknown
Bubbles	Potentially low, because it reuses technology that's already mass produced
Thermo-Optics	Potentially very low, as planar technology lends itself to mass production. Some vendors anticipate that polymer switches will be cheap enough for access networks.

Holograms	Not disclosed
Liquid Gratings	Potentially low cost because a single device performs the function of two or more in alternative technologies. For instance, the projected price of a 4x4 device is $1,500.
Acousto-Optics	At least one vendor of acousto-optic lab equipment says the technology is too expensive for general telecom applications.

3.2.3.2.7. Power consumption

Technology	**Key characteristics: Power consumption**
MEMS	Difficult to quantify, but is thought to be higher than other types of optical switch fabric, and considerably less than for electrical switch cores.
Liquid Crystal	Very low for "bistable" crystals -- those that only need a current to shift them from one stable state to another. Crystals that only have one stable state need a continuous voltage applied to them, but still use a lot less power than MEMS. Heating the crystals to improve switching speeds can bump up power requirements.
Bubbles	Unknown.
Thermo-Optics	Polymer-based switches require very low switching power, typically 5 milliwatts. Silica switches consume about 100 times more power.
Holograms	Trellis's 240x240 port switch consumes less than 300 watts. High voltages are required, placing demands on the electronic supply equipment.
Liquid Gratings	Typically 50 milliwatts
Acousto-Optics	Unknown

3.3 Reference

[1] T. Fjelde, et al, " Novel Scheme for Efficient Label-Swapping Using Simple XOR Gate", Proceeding of ECOC'2000, Vol. 4, pp. 63-64, September 2000.

[2] N. Wada, et al, " Photonic Packet Switching based on Multi-wavelength Label Switching Using Fiber Bragg Gratings", ECOC'2000, paper P10.4.6, Sep. 3-7, 2000, Munich, Germany.

[3] A. Carena, et al, " OPERA: An Optical Packet Experimental Routing Architecture with Label Swapping Capability", IEEE/LEOS Journal of Lightwave Technology. Vol. 16, No. 12, pp. 2135-2145, December 1998

[4] Y. G. Wen, L. K Chen and F. Tong, " Fundamental Limitation and Optimization on Optical Code Conversion for WDM Packet Switching Networks", Proceeding of OFC'2001, paper TUv-5, March 17-22, California, USA.

[5] H. Sotobayashi, et al, " Broadcast-and–select OCDM/WDM network using 10Gbit/s spectrum-sliced supercontinuum BPSK pulse code sequences", IEE Electronics Letters, Vol. 35, NO. 22, October 1999, pp. 1966-1967.

[6] Chih-Hong Eyoh, et al, " Architecture of ATM Transit Switching Using Optical CDMA Technique", International Conference on Information, Communications and Signal Processing, ICICS'97, pp.873-877, Singapore, 9-12 September 1997.

[7] Y.G. Wen, L. K. Chen, K. P. Ho and F. Tong, " An All-Optical Code Converter Scheme for OCDM Routing Networks", ECOC'2000, paper P4.5, September 3-7, 2000, Munich Germany.

[8] F. R. K. Chung, et al, " Optical Orthogonal Codes: Design, Analysis and Applications", IEEE Transaction of Information Theory, Vol. IT-35, pp. 595-604, May 1989.

[9] A. S. Holmes, et al, " All-optical CDMA using Quasi-Prime Codes", IEEE/LEOS Journal of Lightwave Technology, Vol. 10, pp. 279-286, February 1992

[10] W. C. Kwong and P. R. Prucnal, " Programmable ultrafast all-optical code-division multiple access networks", Proceeding of OFC'92, pp. 134, San Jose, CA, USA, February 1992.

[11] P. R. Prucnal, et al, " Spread Spectrum fiber-optic local area network using optical processing", IEEE/LOES Journal of Lightwave Technology, Vol. LT-4, pp. 547-554, May 1986.

[12] W. C. Kwong, et al, " Demonstration of a programmable ultrafast all-optical code-division mulple access network", Proceeding of CLEO'92, pp. 44-45, Anaheim, CA, USA, May 1992.

[13] P. Ohlen, L. Thylen and E. Berglind, " Dispersion Limits in 10Gb/s standard fiber systems using nonlinear optoelectronics repeaters", IEEE Photonics Technology Letters, Vol. 9, No. 8, pp. 1155-1157, August 1997.

[14] N. Wada, H. Sotobayashi and K. Kitayama, " Error-free 100km transmission at 10Gb/s in optical code division multiplexing system using BPSK picosecond-pulse code sequence with novel time-gating detection", Electronics Letter, Vol. 35, pp. 833-834, 1999.

[15] Ding Wang, et al. "Nonlinear optical loop mirror based on standard communication fiber", IEEE/LEOS Journal of Lightwave Technology, Vol.15 No. 4, pp. 642 –646, April 1997.

[16] J.P.; Prucnal, et al. " A Terahertz optical asymmetric demultiplexer (TOAD)", IEEE Photonics Technology Letters, Vol. 5 No. 7, pp. 787 –790, July 1993.

[17] Patel, N.S.; Rauschenbach, K.A.; Hall, K.L., "40-Gb/s demultiplexing using an ultrafast nonlinear interferometer (UNI)", IEEE Photonics Technology Letters, Vol. 8, No. 12, pp. 1695 –1697, Dec. 1996.

[18] Nakamura S., et al, " Error-free all-optical data pulse regeneration at 84 Gbps and wavelength conversion with Symmetric Mach-Zehnder all-optical switches", Proceeding of OAA'2000, PDP4.

[19] "Optical Switching Fabric", Report, October 30, 2000, http://www.lightreading.com/document.asp?site=lightreading&doc_id=2254.

[20] Shun Yao, et al, "Advances in Photonic Packet Switching: An Overview", IEEE Communication Magazines, pp. 84-94, February 2000.

Chapter 4

Scalability of OOC-based MPLS network

4.1 Limitation on Label Switching Capacity

The limitation on label switching capacity occurs when MAI exceeds the threshold value of the TGIT device, generating a "ghost" pulse or an encoding error in the code-regeneration stage. The rate at which this error occurs is termed as the Code Conversion Error Rate (CCER). CCER is mainly due to the MAI, and we neglect other effects and assume the other three stages of the core router have ideal performance in this study. To derive the CCER, we assume:

1. There are M co-propagation code channels that employ M quasi-orthogonal codes in N wavelengths;
2. All channels have identical average input power at each decoder element;
3. Every channel has identical bit rate; and
4. The path length difference in the decoder is longer than the sources' coherence length.

The transmitting signal $S_n(t)$ for the data labeled with n^{th} code is

$$S_n(t) = s_n d_n(t) C_n(t), \tag{1}$$

where s_n, $d_n(t)$, and $C_n(t)$ correspond to the respective transmitted optical intensity, binary bit of the transmitting signal, and the n^{th} OOC. $d_n(t)$ is given by

$$d_n(t) = \sum_{l=-\infty}^{\infty} d_l^{(n)} P_T(t - lT), \tag{2}$$

where $d_l^{(n)}$ is the l^{th} data bit of the n^{th} label that takes on ZERO or ONE (on-off keying) with equal probability, and $P_T(t)$ is the rectangular pulse with duration T. The OOC, with length L and weight W, is given by

$$C_n(t) = \sum_{j=-\infty}^{\infty} A_j^{(n)} P_{T_c}(t - jT_c). \tag{3}$$

Here, $P_{Tc}(t)$ is the rectangular pulse of duration T_c (chip duration) and $A_j^{(n)}$ is the n^{th} code sequence, which is represented by binary optical pulses (0, 1) with period/code length $L=T/T_c$, i.e., $A_{j+L}^{(n)} = A_j^{(n)}$.

Summing all labeled data, the wavelength demultiplexed signal after the first demultiplexer is

$$r(t) = \sum_{n=1}^{M} S_n(t-\tau_n) = \sum_{n=1}^{M} d_n(t-\tau_n) C_n(t-\tau_n), \tag{4}$$

where τ_n is the corresponding delay for individual data, $s_n = 1$ $(1 \le n \le M)$ is assumed for simplicity, and other parameters are normalized.

Consider any given channel (take n=1 and τ_1=0 for convenience), the decoder is equivalent to an optical matched filter with output Z at time T given by

$$Z = \frac{1}{T_c} \int_0^T r(t) C_1(t) dt = d^{(1)} W + I_1 + N_T, \tag{5}$$

where T and T_c are the time duration of data bit and code chip, W is the code weight of the first channel C_1, and $d^{(1)}$ is the detected data bit that can take on either ZERO or ONE with equal probability. In this equation, $d^{(1)}W$ is the desired signal term, $I_1 = \sum_{n=2}^{M} I_n^{(1)}$ describes the MAI corresponding to the interference from other channels, and N_T is the thermal noise with zero mean and variance σ_T^2.

Note that I_1 is the sum of (M-1) interference signals $I_n^{(1)}$ where each $I_n^{(1)}$ is a random variable with mean $\mu_{I_n^{(1)}}$ and variance $\sigma^2_{I_n^{(1)}}$. Without loss of generality, $I_n^{(1)}$ $(2 \le n \le M)$ are assumed independently and identically distributed random variables. Then the mean μ_{I_1} and the variance $\sigma^2_{I_1}$ of the total MAI I_1 are given as

$$\mu_{I_1} = (M-1)\mu, \tag{6}$$

$$\sigma^2_{I_1} = (M-1)\sigma^2, \tag{7}$$

where $\mu = \mu_{I_n^{(1)}}$ and $\sigma^2 = \sigma^2_{I_n^{(1)}}$ for $2 \le n \le M$. Therefore, the mean μ_Z and the variance σ_Z^2 of the Gaussian random variable Z are

$$\mu_Z = d^{(1)}W + (M-1)\mu, \tag{8}$$

$$\sigma_Z^2 = (M-1)\sigma^2 + \sigma_T^2. \tag{9}$$

The probability density function (PDF) for Z is then

$$\rho_Z(Z) = \frac{1}{\sqrt{2\pi\sigma_Z^2}} \exp\left(-\frac{(Z-\mu_Z)^2}{2\sigma_Z^2}\right). \tag{10}$$

Conceptually, the CCER can be defined as

$$PE_{CCER}(Th) = \Pr(d^{(1)}=0)\Pr(Z = I_1 + N_T \ge Th) + \Pr(d^{(1)}=1)\Pr(Z = W + I_1 + N_T \le Th)$$
$$= \frac{1}{2}\left[\int_{Th}^{\infty} \rho_Z\left(Z \mid d^{(1)}=0\right)dZ + \int_{-\infty}^{Th} \rho_Z\left(Z \mid d^{(1)}=1\right)dZ\right] = \frac{1}{4}\left[erfc\left(\frac{Th-(M-1)\mu}{\sqrt{2}\sigma_Z}\right) + erfc\left(\frac{W+(M-1)\mu-Th}{\sqrt{2}\sigma_Z}\right)\right] \tag{11}$$

where *Th* is the effective threshold value of the TGIT device, and *erfc*(*) is the complementary error function, defined as [1],

$$erfc(x) = \frac{2}{\sqrt{\pi}} \int_x^{\infty} e^{-t^2} dt. \tag{12}$$

To avoid lengthy calculations of all possible cross-correlation functions of a certain OOC set, the CCER bounds under two extreme conditions are analyzed. One is the chip synchronous case corresponding to the upper bound, and the other is the ideal chip asynchronous case, corresponding to the lower bound [2,3].

4.1.1 Upper Bound

For the chip synchronous case where all channels are synchronous in chip level, the variance of the MAI can take the maximum value, and this will give highest CCER [2]. For this case, the mean and variance of the individual interference signal $I_n^{(1)}$ are

$$\mu = \frac{W^2}{2L}, \tag{13}$$

and

$$\sigma^2 = \frac{W^2}{2L}\left(1-\frac{W^2}{2L}\right). \tag{14}$$

Therefore, the upper bound of CCER is given by

$$PE_{CCER}(Th) = \frac{1}{4}erfc\left(\frac{Th-(M-1)\frac{W^2}{2L}}{\sqrt{2\left[\sigma_T^2+(M-1)\frac{W^2}{2L}\left(1-\frac{W^2}{2L}\right)\right]}}\right)+\frac{1}{4}erfc\left(\frac{W+(M-1)\frac{W^2}{2L}-Th}{\sqrt{2\left[\sigma_T^2+(M-1)\frac{W^2}{2L}\left(1-\frac{W^2}{2L}\right)\right]}}\right). \tag{15}$$

4.1.2 Lower Bound

For the ideal chip asynchronous case where all channels are asynchronous, the variance of the MAI can reach the minimum value, and this will give the lowest CCER [2]. For this case, the mean and variance of $I_n^{(1)}$ are given by

$$\mu = \frac{W^2}{2L}, \tag{16}$$

and

$$\sigma^2 = \frac{W^2}{L}\left(\frac{1}{3}-\frac{W^2}{4L}\right). \tag{17}$$

Thus, the lower bound of CCER is given by

$$PE_{CCER}(Th) = \frac{1}{4}erfc\left(\frac{Th-(M-1)\frac{W^2}{2L}}{\sqrt{2\left[\sigma_T^2+(M-1)\frac{W^2}{L}\left(\frac{1}{3}-\frac{W^2}{4L}\right)\right]}}\right)+\frac{1}{4}erfc\left(\frac{W+(M-1)\frac{W^2}{2L}-Th}{\sqrt{2\left[\sigma_T^2+(M-1)\frac{W^2}{L}\left(\frac{1}{3}-\frac{W^2}{4L}\right)\right]}}\right). \tag{18}$$

Using Eq.15 and Eq.18, the CCER's upper and lower bounds are plotted with respect to the threshold value in Figure 4.1, showing similar characteristics for both the upper bound and the lower bound. The combination of the MAI and the thermal noise yields a CCER floor for the proposed code converter. This is shown in Figure 4.2 where the CCER floor (upper bound) is plotted against the number of code channels to illustrate the effects of MAI on the label switching capacity of each switch fabric. For code weights of 5 or 10 and code lengths of 800 or 1500, the

switch fabric can support up to 12 code channels with an acceptable CCER floor of 10^{-9}. To achieve the minimum CCER, we derived the optimum threshold value from Eq.11, yielding

$$Th_{opt} = \frac{W}{2} + (M-1)\frac{W^2}{2L}. \tag{19}$$

The first part of the expression is originated from the OOC's code weight while the latter part is due to the MAI from the co-propagation label/code channels. The dash lines in Figure 4.1 shows the variation of Th_{opt} value versus the number of code channel. For $W = 10$, $L = 1000$, $\sigma_T = 0.01$, the optimum threshold values are 5.35, 5.45 and 5.7 for label numbers of 8, 10 and 15, respectively. These values are ~5, the ideal threshold for system without MAI. Moreover, these optimum threshold values increase with increasing number of co-propagation label/code channels, due to more MAI contribution from increasing number of label/code as manifested in Eq.19.

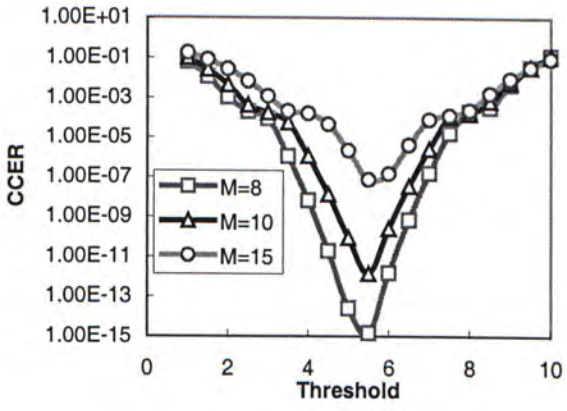

(a) Upper Bound

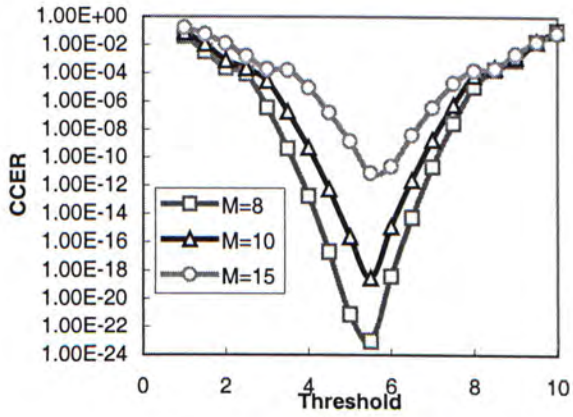

(b) Lower Bound

Figure 4.1 The code conversion error rate (CCER) against the threshold value: (a) upper bound and (b) lower bound. $W = 10$, $L = 1000$, σ_n=0.01, and $M = 8$, 10 and 15 as shown.

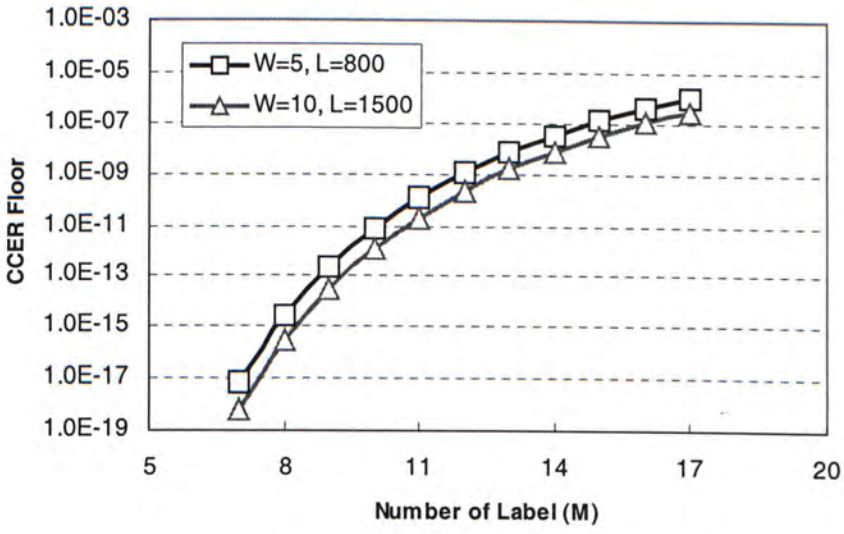

Figure 4.2 The CCER floor of upper bound versus the number of label channel. The traces converge to 0.5.

4.2 Limitation on Switching Cascadability

The scalability of the photonic OOC-based MPLS network is critically determined by the cascadability of optical switch fabric, whose performances should be determined by the implementation of the fabric. For our proposed core router, the cascadability could be degraded by the non-deal performance of the optical space switch and the TGIT device. For example, the finite crosstalk suppression ratio (ε) of the optical space switch induces inter-channel coherent and incoherent crosstalk, and the limited on/off ratio (α) of the TGIT device induces the residue intensity of MAI and sidelobes. Others disturbances such as fiber dispersion [4] and intersymbol interference [5] contribute insignificantly to fabric performance because the TGIT device can combat the detrimental effects of chromatic dispersion and suppress the sidelobes of the autocorrelation and the cross-correlations [6]. Such effects will not be discussed here. In the following, the detrimental effects of the finite crosstalk suppression ratio (ε) of the optical space switch and the limited on/off ratio (α) of the TGIT device will be investigated with the assumption of ideal performance for other devices.

4.2.1. Limit Induced by the Inter-channel Crosstalk

Inter-channel crosstalks are generated from the intrinsic non-ideal crosstalk suppression ratio of the switching gate in the switching fabric. The crosstalks can be classified into two categories, coherent crosstalk (on the same wavelength, within the electrical bandwidth of the main channel) and incoherent crosstalk (on a different wavelength) [7]. For the aforementioned optical switch fabric, the maximum number of coherent crosstalk contributions is M - 1 and the maximum number of incoherent crosstalk contributions is $2(N - 1)$ [8]. Crosstalks can induce a timing jitter that will accumulate in cascading nodes, eventually degrading the system performance in terms of BER. Thus, a certain SNR is required at the input of cascaded switching nodes to guarantee an acceptable BER at the final stage. In [8], the required SNR at

the input of cascaded optical cross connects (OXC) with wavelength conversion function is given as

$$SNR_{req} = \frac{1}{4} \Big/ \left[\frac{\kappa^2}{8hq_0^2} - \frac{\sigma_c^2 + \sigma_i^2}{A^2} \right], \tag{20}$$

where κ is the slope of the rising edge of the signal, h is the number of cascaded nodes, A is the amplitude of the signal, q_0 is the Q-value for an acceptable BER, and σ_c^2 and σ_i^2 are the variances of the coherent and incoherent crosstalk, respectively. For our case, the variances of both coherent and incoherent crosstalk in the worst-case scenario (same polarizations) are given by

$$\sigma_c^2 = \frac{1}{2}(M-1)\varepsilon\left(1+\left(\frac{1}{2}(M-1)+1\right)\varepsilon\right)A^2, \tag{21}$$

$$\sigma_i^2 = \frac{1}{2}\cdot 2(N-1)\varepsilon^2 A^2 \quad , \tag{22}$$

where ε is the crosstalk suppression ratio of the optical space switch fabric. Thus, the required SNR is

$$SNR_{req} = \frac{1/4}{\frac{\kappa^2}{8hq_0^2} - \frac{1}{2}\left((M-1)\varepsilon\left(1+\left(\frac{1}{2}(M-1)+1\right)\varepsilon\right)+2(N-1)\varepsilon^2\right)}. \tag{23}$$

From Eq.23, the crosstalk-induced power penalty is

$$\delta(h) = 10\log\frac{\frac{\kappa^2}{8hq_0^2}}{\frac{\kappa^2}{8hq_0^2} - \frac{1}{2}\left((M-1)\varepsilon\left(1+\left(\frac{1}{2}(M-1)+1\right)\varepsilon\right)+2(N-1)\varepsilon^2\right)}. \tag{24}$$

From Eq.24, the crosstalk-induced power penalty versus the number of cascaded nodes is plotted in Figure 4.3 for various N and ε. In the figure, we assume $M = N$, and $q_0 = 6$ for $BER = 10^{-9}$. The crosstalk-induced power penalty increases with more cascaded switch nodes. Thus, under different power penalty criteria, the maximum number of cascaded nodes can be derived, given by

$$h(\delta)=\frac{\kappa^2}{8q_0^2}\cdot\frac{10^{\frac{\delta}{10}}-1}{10^{\frac{\delta}{10}}}\cdot\frac{1}{\frac{1}{2}\left((M-1)\varepsilon\left(1+\left(\frac{1}{2}(M-1)+1\right)\varepsilon\right)+2(N-1)\varepsilon^2\right)}. \tag{25}$$

The results are shown in Figure 4.4, showing the maximum number of nodes as a function of the crosstalk suppression ratio for various N and δ. For a 1-dB power penalty criterion [9], up to 20 switch nodes can be cascaded, each with a switch size of 64 labels (8-code/8-wavelength) and 45-dB crosstalk suppression. Table I shows the number of cascaded nodes under different network parameters. From the table, the number of channels (code*wavelength) and the crosstalk suppression ratio are the two key constraints limiting the cascadability of the proposed switch fabric. Under the same power penalty criterion, the maximum number of supportable cascaded nodes increases with the increase of crosstalk suppression ratio, but reduces with increasing number of code/wavelength channels.

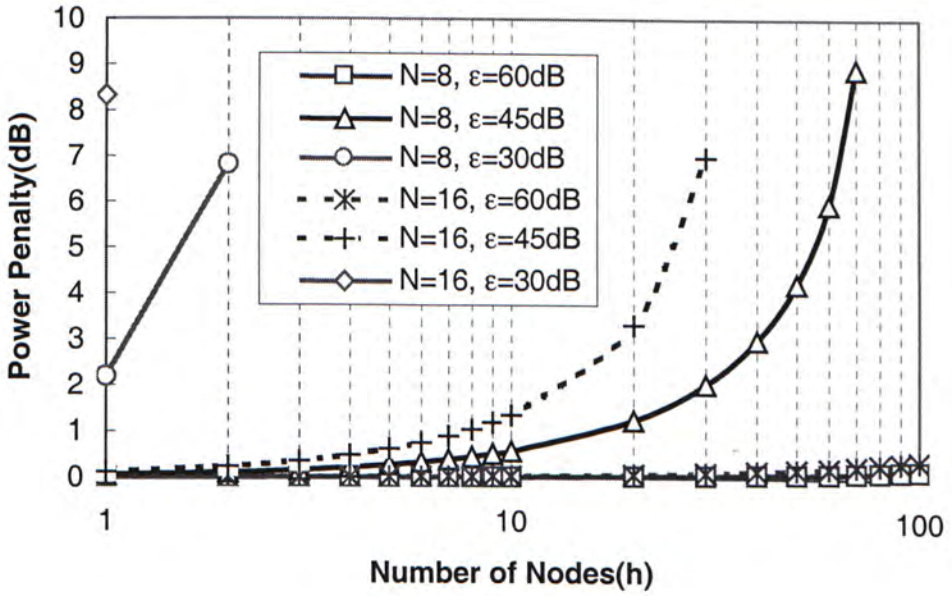

Figure 4.3 The crosstalk-induced power penalty (δ) against the number of the cascaded nodes in the code-based MPLS routing networks. q_0 is set to 6 for the final node with a BER 10^{-9}, and M is set equal to N for simplicity.

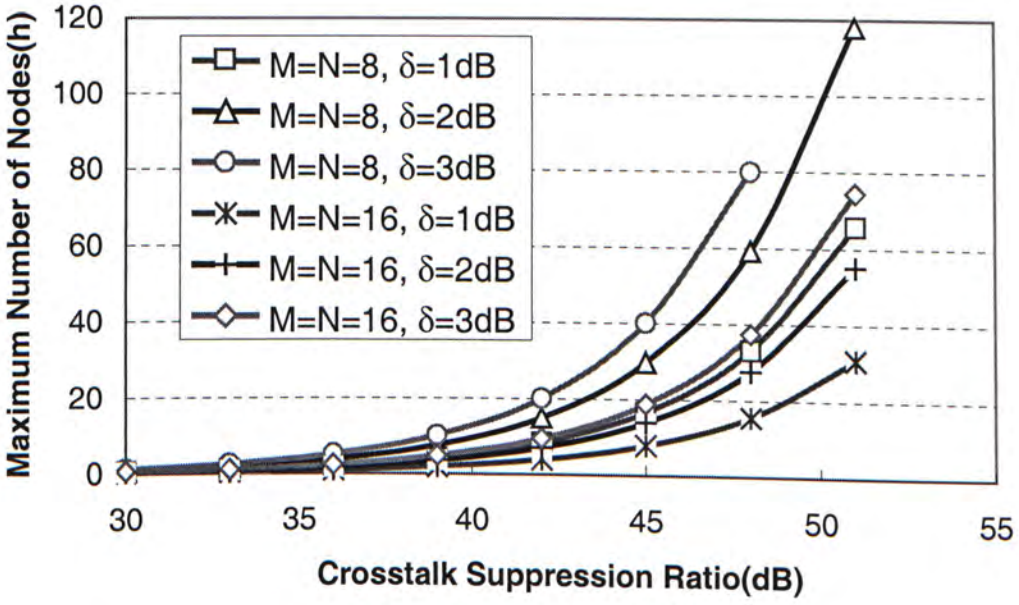

Figure 4.4 The maximum number of nodes versus the crosstalk suppression ratio (ε) of the optical space switch. Different power penalty criteria (δ=1dB, 2dB and 3dB) are assumed.

4.2.2 Limits Induced by the Residual Intensity of MAI and Sidelobes

In Chapter 3, the effects of the MAI on label switching capacity are analyzed with the assumption that ideal threshold device with an infinite on/off ratio are used in the switch fabric. However, practical device exhibits a non-zero output even for input signal below the set threshold. The reported on/off ratio α of SMZI-based threshold device is limited [10]. The residual output will limit the cascadability of the photonic code-based MPLS network.

Figure 4.5 shows the influence of MAI on the cascadability. The code chip patterns after each processor are shown in the circles. For the worst case, we assume that data bits in all labeled channels are ONE. Derived in Appendix 4.3.1, after Node K, the normalized intensities of residue chips (denoted as 2,4,6) and desired chips (denoted as 1,3,5) are given by

$$I_1 = I_3 = I_5 = 1, \tag{26}$$

$$I_2 = \sum_{i=1}^{k} \frac{\alpha^{i-1} W^{2(i-1)} \left[(M-1)\mu + 1\right]}{\left[W + (M-1)\mu\right]^i}, \tag{27}$$

$$I_4 = \sum_{i=1}^{k} \frac{\alpha^{i} W^{2(i-1)} \left[(M-1)\mu + 1\right]}{\left[W + (M-1)\mu\right]^i}, \tag{28}$$

$$I_6 = \sum_{i=1}^{k} \frac{\alpha^{i} W^{2i-1} \left[(M-1)\mu + 1\right]}{\left[W + (M-1)\mu\right]^i}. \tag{29}$$

From equation (27)-(29), the intensity of residue chip 2, 4 and 6 is the summation of a geometric series and converges to the following values as k approaches infinite,

$$I_2 = \frac{(M-1)\mu + 1}{W + (M-1)\mu - \alpha W^2}, \tag{30}$$

$$I_4 = \frac{\alpha\left[(M-1)\mu + 1\right]}{W + (M-1)\mu - \alpha W^2}, \tag{31}$$

$$I_6 = \frac{\alpha W\left[(M-1)\mu + 1\right]}{W + (M-1)\mu - \alpha W^2}. \tag{32}$$

To show the convergence of the residue chip, the normalized intensity of chip 6 is plotted in Figure 4.6 against the cascaded node number. From the figure, in general, the residual intensity of chip 6 converges very quickly. Moreover, the code weight W and the on/off ratio α determine the convergence rate and the converged intensity of the residue chips. The higher the on/off ratio α, the faster the convergence, and the lower the intensity of residue chips. Meanwhile, with the reduction of the code weight, the convergence rate would increase and the normalized intensity would decrease.

After the intensity of residue chips converges ($h \to \infty$), most important factors that determine the quality of transmission are the number of the co-propagation code channels per wavelength and the on/off ratio α. From equation (32), Figure 4.7 shows the relation between the residue chip intensity and the code number per wavelength channel. The normalized residual intensity increases with more label channels. With the same OOC design, the residual power is determined by the on/off ratio α. By the 5% residue power criterion (Derived in Appendix 4.3.2), with α =10 dB (W=5, L=1000), the residual intensity is unacceptable for any number of code channel (M) per wavelength. Thus it cannot support any label channel. While for α=15 dB (W=5, L=1000), the system can support up to 24 code channels per wavelength. In addition, if the code weight is reduced, it can support more code channels. For an OOC(W, L) code set, the number of code is bounded by $M_x = (L-1)/W(W-1)$ [11]. This equation shows that enough labels can be designed to cater for the increasing demand of OOC quota. Specifically, the converged normalized power of residue chips versus α is plotted in Fig. 4.8. From the figure, 15 dB is the minimum effective on/off ratio required with the 5% residue power criterion. With a two-stage TGIT architecture, the on/off ratio of every individual stage can be relaxed by 4-5 dB [12] since a quasi-digital transfer function obtained by cascading two stage MZI makes the total effective on/off ratio α larger [13].

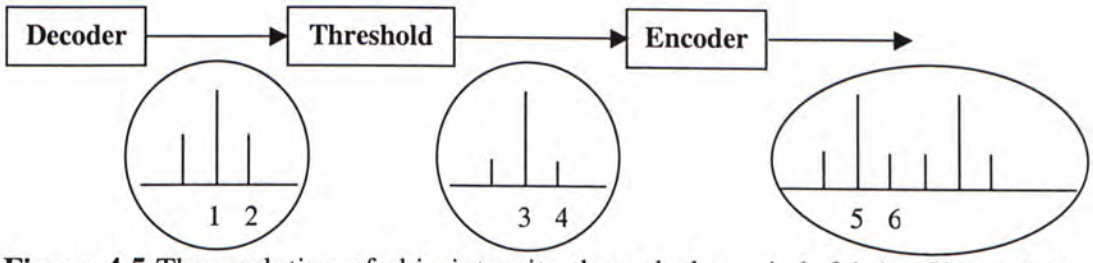

Figure 4.5 The evolution of chip intensity through the switch fabric. Chip 1 is the desired auto-correlation peak, chip 2 is the MAI; Chip 3 is normalized desired peak and chip 4 is the output of residue Chip 2 after the threshold device; Chip 5 is the desired encoded ONE, Chip 6 is the encoded ZERO.

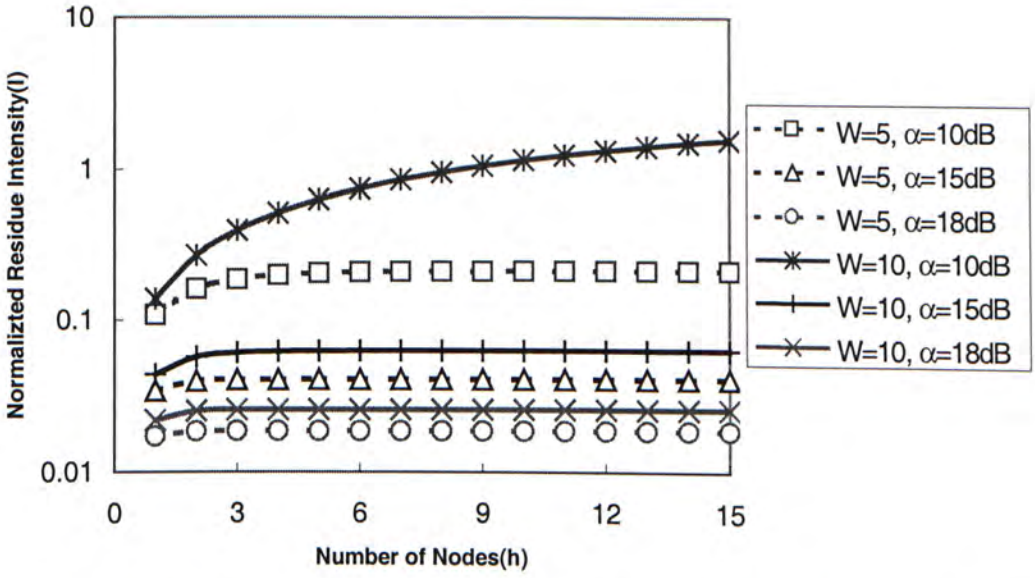

Figure 4.6 The normalized residue intensity of the residue chip 6 versus the number of cascaded nodes. Difference gate suppression ratio (α=10, 15, 18dB) and code weight (W = 5,10) are assumed for the same code length (L = 1000).

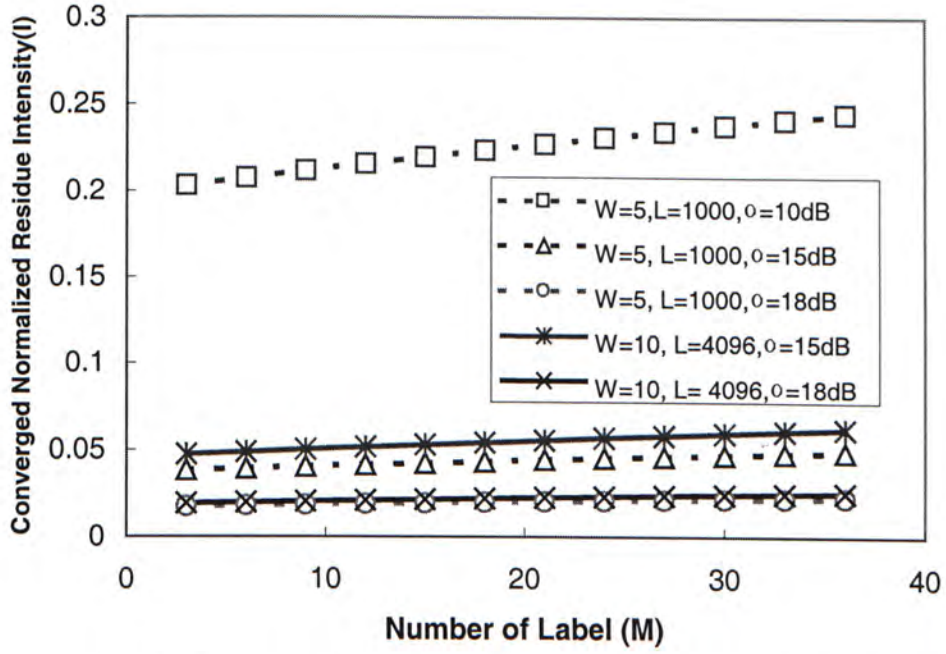

Figure 4.7 The converged normalized intensity (I) of residue chip 6 versus the number of label channels (M).

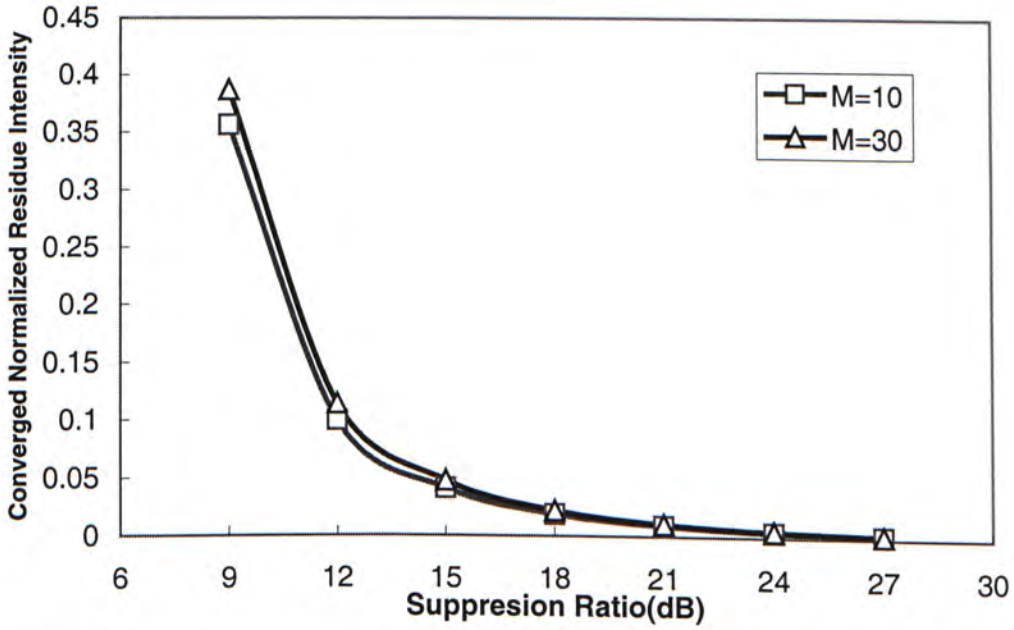

Figure 4.8 The converged normalized intensity (I) of residue chips versus the suppression ratio α. For simulation, $W = 5$, $L = 1000$, $M_x = 50$.

4.3 Appendix

4.3.1 Derivation of Chip Intensity

Without loss of generality, we assume the incoming (prior to a decoder) code chip intensity is normalized to 1 at any node. Fig. 4.5 illustrates the evolution of chip intensity of the desired and residue chips through an optical switch fabric. From the figure, after the decoder, the intensity of chip 1 (the desired chip) is $W+(M-1)\mu$, and the intensity of chip 2 (the residue chip) is $(M-1)\mu+1$ for the worst case (largest possible interference). W is the code weight of the OOC, M is the number of co-propagation codes, and μ is the mean MAI value from other code channels. After normalization, the intensity of chip 1 is 1 and chip 2 is $\left((M-1)\mu+1\right)/\left(W+(M-1)\mu\right)$. These outputs are fed into the TGIT device with an on/off ratio α to suppress the residue chips. After the thresholding and normalization, the intensity of chip 3 (corresponding to chip 1 prior to the threshold device) is 1, and the intensity of chip 4 (corresponding to chip 2 prior to the threshold device) is $\alpha\left((M-1)\mu+1\right)/\left(W+(M-1)\mu\right)$. The outputs are fed into an encoder where a new code is generated. Again, through normalization, the intensity of desired chip 5 is 1, and that of residue chip 6 is $\alpha W\left((M-1)\mu+1\right)/\left(W+(M-1)\mu\right)$.

By the same approach, the normalized intensities of the individual chip (residue and desired) are derived in the following.

At node 1:

$I_1 = I_3 = I_5 = 1$,

$$I_2 = \frac{(M-1)\mu+1}{W+(M-1)\mu},$$

$$I_4 = \frac{\alpha\left[(M-1)\mu+1\right]}{W+(M-1)\mu},$$

$$I_6 = \frac{\alpha W\left[(M-1)\mu+1\right]}{\left[W+(M-1)\mu\right]}.$$

At node 2,

$I_1 = I_3 = I_5 = 1$,

$$I_2 = \frac{\left[(M-1)\mu+1\right]}{\left[W+(M-1)\mu\right]} + \frac{\alpha W^2\left[(M-1)\mu+1\right]}{\left[W+(M-1)\mu\right]^2},$$

$$I_4 = \frac{\alpha\left[(M-1)\mu+1\right]}{\left[W+(M-1)\mu\right]} + \frac{\alpha^2 W^2\left[(M-1)\mu+1\right]}{\left[W+(M-1)\mu\right]^2},$$

$$I_6 = \frac{\alpha W\left[(M-1)\mu+1\right]}{\left[W+(M-1)\mu\right]} + \frac{\alpha^2 W^3\left[(M-1)\mu+1\right]}{\left[W+(M-1)\mu\right]^2}.$$

At node 3,

$I_1 = I_3 = I_5 = 1$,

$$I_2 = \frac{\left[(M-1)\mu+1\right]}{\left[W+(M-1)\mu\right]} + \frac{\alpha W^2\left[(M-1)\mu+1\right]}{\left[W+(M-1)\mu\right]^2} + \frac{\alpha^2 W^4\left[(M-1)\mu+1\right]}{\left[W+(M-1)\mu\right]^3},$$

$$I_4 = \frac{\alpha\left[(M-1)\mu+1\right]}{\left[W+(M-1)\mu\right]} + \frac{\alpha^2 W^2\left[(M-1)\mu+1\right]}{\left[W+(M-1)\mu\right]^2} + \frac{\alpha^3 W^4\left[(M-1)\mu+1\right]}{\left[W+(M-1)\mu\right]^3},$$

$$I_6 = \frac{\alpha W\left[(M-1)\mu+1\right]}{\left[W+(M-1)\mu\right]} + \frac{\alpha^2 W^3\left[(M-1)\mu+1\right]}{\left[W+(M-1)\mu\right]^2} + \frac{\alpha^3 W^5\left[(M-1)\mu+1\right]}{\left[W+(M-1)\mu\right]^3}.$$

...

At node k,

$$I_1 = I_3 = I_5 = 1, \qquad \text{(a)}$$

$$I_2 = \sum_{i=1}^{k} \frac{\alpha^{i-1} W^{2(i-1)} \left[(M-1)\mu + 1 \right]}{\left[W + (M-1)\mu \right]^i}, \tag{b}$$

$$I_4 = \sum_{i=1}^{k} \frac{\alpha^{i} W^{2(i-1)} \left[(M-1)\mu + 1 \right]}{\left[W + (M-1)\mu \right]^i}, \tag{c}$$

$$I_6 = \sum_{i=1}^{k} \frac{\alpha^{i} W^{2i-1} \left[(M-1)\mu + 1 \right]}{\left[W + (M-1)\mu \right]^i}. \tag{d}$$

From equation (b)-(d), for k approaching infinite, the intensities of residue chip 2, 4 and 6 are the summation of an infinite geometric series and converge toward the following values.

$$I_2 = \frac{(M-1)\mu + 1}{W + (M-1)\mu - \alpha W^2} \tag{e}$$

$$I_4 = \frac{\alpha \left[(M-1)\mu + 1 \right]}{W + (M-1)\mu - \alpha W^2} \tag{f}$$

$$I_6 = \frac{\alpha W \left[(M-1)\mu + 1 \right]}{W + (M-1)\mu - \alpha W^2} \tag{g}$$

4.3.2 The 5% residue power criterion

In Fig. 4.5, the 5% residue power criterion is defined to characterize the effect of the residue chips. That is, for the residue chips, intensity below 5% of that of the desired chip is considered acceptable. The reason is illustrated in the following.

For the regenerated code, under ideal conditions, the intensity of the residue chip is 0, and 0.5 is set as the virtual threshold to decide the validity of the code. But with non-ideal threshold device and the cascading effect, the normalized intensity of the residue chip is now given by equation (g), where the normalized intensity of desired chip is 1. From Fig. 4.9, with a Gaussian thermal noise added to every individual chip, the residue chip is subject to a Gaussian distribution with mean I_6 and variance σ^2. Thus, its probability distribution function (PDF) is

$$f(x) = \frac{1}{\sqrt{2\pi\sigma^2}} e^{\frac{(x-I_6)}{2\sigma^2}} \qquad \text{(h)}$$

Therefore, the probability that a residue chip is determined to be ONE, which is denoted by shaded area in Fig. 4.9, is

$$P(I_6) = \int_{0.5}^{\infty} f(x)dx = \frac{1}{2} erfc\left(\frac{0.5 - I_6}{\sqrt{2}\sigma}\right) \qquad \text{(i)}$$

Related to the requirement of network quality of service (QoS), 10^{-9} is assumed acceptable for this probability. Thus, from equation (i), the normalized intensity of the residue chip I_6 is 0.05. This gives rise to the 5% residue power criterion.

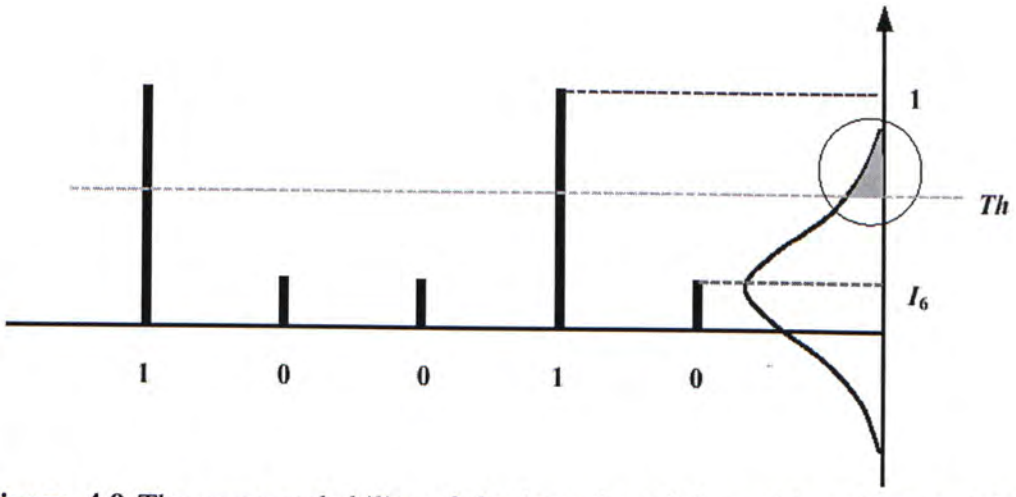

Figure 4.9 The error probability of the intensity of the residue chips and the desired chips. The horizontal coordinate shows the chip pattern of the regenerated code, the vertical coordinate shows the probability distribution of the intensity of the individual chips.

4.4 Reference

[1] B.E.A. Saleh and M. Teich, "Fundamentals of Photonics", Wiley, New York, 1991, Chap. 11.

[2] J. A. Salehi, "Code Division Multiple-Access Techniques in Optical Fiber Networks—Part I: Fundamental Principles", IEEE transactions on communications, Vol.37, No. 8, pp.824-833, August 1989.

[3] J. A. Salehi, and C. A. Brackett, " Code Division Multiple-Access Techniques in Optical Fiber Networks- Part II: Systems Performance Analysis", IEEE Transactions on Communications, Vol. 37, No. 8, pp. 834-842, August 1989.

[4] P. Ohlen, L. Thylen, and E. Berglind, " Dispersion limits in 10gb/s standard fiber systems using nonlinear optoelelctronic repeaters", IEEE Photonic Technology of Letters, Vol. 9, No. 8, August 1997, pp. 1155-1157.

[5] R. J. S. Pederson, et al, " Cascadability of a nonblocking WDM crossconnect based on all-optical wavelength converters for routing and wavelength slot interchanging", Electronic Letters, Col. 33, No. 19, pp. 1647-1648, September 1997.

[6] N. Wada, H. Sotobayashi, and K. I. Kitayama, "Error-free 100km transmission at 10Gbit/s in optical code division multiplexing system using BPSK picosecond-pulse code sequence with novel time-gating detection", Electronics Letter, Vol. 35, pp. 833-834, 1999.

[7] K.-P. Ho, C.-K. Chan, F. Tong, and L. K. Chen, ``Exact Analysis of Homodyne Crosstalk Induced Penalty in WDM Networks," in SPIE's Asia Pacific Symposium on Optoelectronics `98: Optical Fiber Communication, Taipei, Taiwan, July 9-11, 1998, SPIE vol. 3420, pp. 72-77.

[8] P. Ohlen, " Noise and Crosstalk Limitations in Optical Cross-Connects with Reshaping Wavelength Converters", Journal of Lightwave Technology", Vol. 17, No. 8, pp. 1294-1301, August 1999.

[9] Yong-gang Wen, Lian-kuan Chen, Keang-Po Ho, Frank Tong and Wai-shan Chan, "Performance Verification of a Variable Bit Rate Limiter for On-Off-Keying (OOK) Optical systems", IEEE/OSA JOURNAL OF LIGHTWAVE TECHNOLOGY, Vol. 18, No. 6, June 2000, pp.779-786.

[10] S. Nakamura, K. Tajima, and Y. Sugimoto, "High-repetition operation of a symmetric Mach-Zehender all-optical switch", Applied Physics Letters 66(19), pp. 2457-2459, May 1995.

[11] Hossam M. H. Shalaby, " Maximum Achievable Number of Users in Opitcal PPM-CDMA Local Area Networks", IEEE Journal of Lightwave Technology, Vol. 18, NO. 9, September 2000, pp. 1187-1288.

[12] B. Mikkelsen, et al., " Impact on traffic and transmission performance of all-optical wavelength converters placed at the network interface or in OXCNs", OFC'97, paper WD6.

[13] A. J. Poustie, et al, " Storage threshold and amplitude restoration in an all-optical regenerative memory", Optics Communications 146(1998), pp. 262-267.

Chapter 5

Conclusion

5.1 Summary of the Thesis

In this thesis, an optical MPLS network using OOC as label is proposed with the architecture of core router based on all-optical code converter. The fundamental limits on scalability of the proposed core router, including the label capacity and the switch cascadability, are investigated with close-form solutions derived.

Chapter 2 presented an overview of optical MPLS network and optical label schemes. A generic OMPLS network is proposed with its layer infrastructure. The optical label schemes include (1) time-division label scheme, (2) wavelength-division label scheme, (3) frequency-division label scheme and (4) code-division label scheme.

Chapter 3 provided the details of implementing the all-optical OMPLS core router. Basically, it is a four-stage code converter: decoder, threshold device, optical space switch and encoder. The implementation issues of these devices are presented in this chapter, including different approaches and comparison among these approaches.

Chapter 4 presented the scalability of the photonic OOC-based MPLS network, whose performances should be determined by the implementation of the fabric. For our proposed core router, the cascadability could be degraded by the non-deal performance of the optical space switch and the TGIT device. For example, the finite crosstalk suppression ratio (ε) of the optical space switch induces inter-channel coherent and incoherent crosstalk, and the limited on/off ratio (α) of the TGIT device induces the residue intensity of MAI and sidelobes. In this chapter, the detrimental effects of the finite crosstalk suppression ratio (ε) of the optical space switch and the limited on/off ratio (α) of the TGIT device are investigated with the assumption of ideal performance for other devices. By the criteria of 1-dB power-penalty and 5% residue intensity, the numerical simulations show that the network

can support up to 20 consecutive nodes for 64-label (8-wavelength, 8-code) switch fabric with 45-dB crosstalk suppression.

5.2 Future work

For future work, it could be classified into two aspects, one is the experimental work, and the other is theoretical work.

Due to the device availability problem, a fully functional core router based on OOC MPLS technology was not implemented. For future work, an all-optical four-stage code converter can be implemented, and the testbed of OOC-based OMPLS network can be setup hereafter. And, the performance of the testbed can be verified with the implementation of a switching node.

We have investigated the scalability of the proposed OOC-based OMPLS network in this thesis. The cascadability could be degraded by the non-deal performance of the optical space switch and the TGIT device. For example, the finite crosstalk suppression ratio (ε) of the optical space switch induces inter-channel coherent and incoherent crosstalk, and the limited on/off ratio (α) of the TGIT device induces the residue intensity of MAI and sidelobes. Others disturbances such as fiber dispersion and intersymbol interference can also contribute detrimentally to fabric performance. For future work, the effects of these issues can be investigated in more details. Another interesting topic is the code allocation algorithm for better throughputs.

Appendix: Publication Lists

1. November 1999

Title: Performance Verification of a Variable Bit Rate Limiter for On-Off-Keying (OOK) Optical Systems

Authors: Yong-Gang Wen, Lian-Kuan Chen, Keang-Po Ho, Frank Tong and Wai-Shan Chan

Publisher: IEEE/OSA JOURNAL OF LIGHTWAVE TECHNOLOGY, Vol. 18, No. 6, June 2000, pp.779-786

Abstract: A close-form analytical expression is obtained for the performance study of a Bit Rate Limiter (BRL). Both Bit-Error-Rate (BER) and power penalty are derived for different BRL modulation signals and modulation formats using a random signal model. We also present ways to improve the BRL performance and to eliminate the BRL-induced crosstalk, by using an optimal BRL modulation index and a specific BRL modulation signal, respectively. The analytical expression is found to match well with the experimental measurements.

2. March 2000

Title: An All-optical Code Converter Scheme For OCDM Routing Networks

Authors: Yong-Gang Wen, Lian-Kuan Chen, Keang-Po Ho and Frank Tong

Publisher: ECOC'2000, paper P4.5, Sep 3-7, 2000, Munich Germany

Abstract: A novel all-optical code converter scheme using a TOAD-based architecture is proposed for OCDM routing networks. Theoretical analysis of BER and power penalty is given and shows less than 0.22 dB extinction-ratio-induced power penalty.

3. October 2000

Title: Fundamental Limitation and Optimization on Optical Code Conversion for WDM Packet Switching Networks

Authors: Y.G. Wen, L.K. Chen and F. Tong

Publisher: Proceeding of OFC'2001, paper TUv-5, March 17-22, California, USA.

Abstract: Fundamental performance limitation originated from multi-access interference on a generic code converter for WDM packet switching networks is derived and analyzed. A closed-form optimal threshold value that yields the lowest code conversion error is also given.

4. November 2000

Title: Fundamental Limits on Scalability of Photonic Code-based Multi-Protocol Label Switching (MPLS) Networks

Authors: Yong-gang Wen, Yu Zhang, Lian-Kuan Chen and Frank Tong

Publisher: Submitted to *JLT*, Paper #5017

Abstract: The fundamental limits on the scalability of optical multi-protocol label switching (OMPLS) networks using optical orthogonal codes (OOC) as labels are investigated in this paper. Based on the proposed four-stage architecture of the optical core router, close-form results for the label switching capacity and the network cascadability are derived. Originated from the intrinsic uni-polar property of OOC, the multi-access interference (MAI) results in a code conversion error rate (CCER) floor for the scheme. Accordingly, the label switching capacity, i. e., the maximum number of supportable code channels per wavelength, is determined by the acceptable CCER floor. Inter-channel crosstalks due to the finite crosstalk suppression ratio of the optical space switch, and the residue intensity of the sidelobes from the decoder due to the limited on/off ratio of the threshold device are also analyzed, and their impacts on cascadability are manifested by close-from expressions. By the criteria of 1-dB power-penalty and 5% residue intensity, our numerical simulations show that the network can support up

to 20 consecutive nodes for 64-label (8-wavelength, 8-code) switch fabric with 45-dB crosstalk suppression.

5. March 2001

Title: A Novel All-Optical Code Converter Scheme For OCDM Routing Networks

Authors: Yong-gang Wen, Lian-Kuan Chen, Keang-Po Ho, and Frank Tong

Publisher: In preparation

Abstract: An all-optical code converter scheme using an SMZI-based architecture is proposed for future optical code-division multiplexed (OCDM) routing networks. Theoretical analysis of BER performance and extinction-ratio-induced power penalty is given and shows less than 0.044 dB extinction-ratio-induced power penalty.